A new method for the automated design of cooling systems in injection molds

Jorge Manuel Mercado-Colmenero [a], Miguel Angel Rubio- Paramio [b], Juan de Juanes Marquez-Sevillano [c], Cristina Martin-Doñate [d*]

[a, b, d] Department of Engineering Graphics Design and Projects. University of Jaen. Spain

[c] Department of Mechanical Engineering. Polytechnical University of Madrid. Spain

*Corresponding Author[d]

Campus Las Lagunillas, s/n. Building A3-210

23071 Jaen (Spain)

Phone: +34 953212821, Fax: +34 953212334

E-mail: jmercado@ujaen.es [a], marubio@ujaen.es [b], juandejuanes.marquez@upm.es [c], cdonate@ujaen.es [d]

Abstract

This paper presents a new method for the automatic design of the cooling system in injection molds, based on the discrete geometry of the plastic part. In a first phase the new algorithm recognizes the discrete topology of the part, obtaining its depth map and detecting flat, concave regions and slender details which are difficult to cool. The algorithm performs an automatic analysis of the heat transfer, taking into account functional parameters, in order to guarantee a uniform cooling of the part. Based firstly on the limit range distance from which the horizontal straight channels lose cooling effectiveness and secondly on the depth map data, the algorithm provides an optimal layout for the cooling system of the part by adapting it to its geometry. By means of adapting the precision of the algorithm to the molded geometry, both horizontal straight channels for low concavity areas and baffle matrixes for concave regions are used. In a second phase, the parameters of the cooling system such as channel diameter, channel separation etc, are dimensioned by means of genetic optimization algorithms. A second genetic optimization algorithm ensures uniformity and balance in the layout of the cooling system for the plastic part. The result is the design of the cooling system for the plastic part with the same performance as the conformal system. A constant distance between the cooling channels and the part surface is maintained, and at the same time the manufacturing of the mold using CNC techniques and traditional metal materials could be achieved. Complementarily, the algorithm performs an interference analysis with other parts of the mold such as the ejection system. The method does not need a subsequent CAE analysis since it takes into account functional and technical parameters related to heat transfer in its design, thus ensuring its functionality. The algorithm is independent of the CAD modeler used to create the part since it performs a recognition analysis of the part surfaces, being able to be implemented in any CAD system. The data obtained in the design can be used additionally in later applications including the automated design of the injection mold.

Keywords: Cooling System, Injection molding, Discrete Geometry, Surfaces geometric recognition, Genetic Optimization

1. Introduction

The plastic injection molding process begins with the injection of the thermoplastic material at a high temperature into the cavity formed by both mold cavities. Once inside the mold the plastic is compacted, cooling until it acquires the solidification temperature that allows the geometry of the piece to be maintained without deformation. The duration of the molding cycle as such is not enough to dissipate the heat of the injected plastic by means of heat conduction through the metal material of the mold. Thus, in order to improve the efficiency of the process, the mold is cooled using a set of hollow channels made in both cavities through which a cooling fluid performs a better heat exchange. At present there are several possibilities in relation to the design of the cooling channels of the plastic injection mold. The choice of design depends mainly on three factors: the geometric characteristics of the plastic part, the size of the mold and the manufacturing technology required by each cooling system. Taking these factors into account, cooling systems can be designed by means of conventional cooling models or conformal systems, adapted to the part geometry. The conventional systems have the advantage of their low cost of manufacture since they use traditional machining techniques. Nevertheless, they have a limited application only to slender parts with flat geometries, and without deep concavities. Unlike traditional cooling channels, the conformal cooling channels maintain a constant distance between the surface of the mold cavities in contact with the part and the cooling circuit, thus obtaining precise temperature control in parts with complex surfaces. The conformal method requires Rapid

Tooling Technologies for the manufacture of mold cavities, with the inconvenience of its lack of functionality in medium size molds for industrial applications. To resolve these problems, the "Milled Groove" and "Array of Baffles" hybrid refrigeration systems take advantage of conformal designs, maintaining a constant distance between the channels and the part, but manufactured with traditional machining processes. The proper choice of the cooling system is fundamental for the uniform transfer of heat in the part, assuming an adequate manufacturing cost. A detailed recognition of the part surface from the first phases of mold design allows detection of its geometric characteristics, which can be decisive for the proper choice of cooling system. While in the automatic analysis of other parts of the mold [1-4] only geometric type parameters have influence, in the design of the cooling system a series of requirements related to the heat transfer in the mold must be fulfilled in parallel. Knowing these parameters and including them as design requirements ensures their good operation regardless of the use of CAE or CFD tools.

The design of the cooling channels layout is currently carried out by experienced designers who usually take as reference a set of geometric criteria based on their experience and related to dimensional values of depth and separation between channels. The design is performed manually by validating the result a posteriori by means of numerical simulation programs. If the result indicates that the design presented does not assure the quality requirements of the part, it is modified again by an iterative trial and error process. This methodology poses several drawbacks, including the large amount of time required by experts who are sometimes not available due to the company's workload, its high level of specialization and the availability of CAE or CFD simulation software. In spite of the importance of rigorously designing the mold cooling system, there are few studies related to obtaining geometric algorithms for the automatic design of the cooling system for injection molds. Most studies focus on conformal design algorithms for later manufacture using rapid-tooling techniques, and these are not valid for use in medium and large industrial molds. Other studies propose algorithms that only take into account geometric design criteria, do not automate the whole design process, or are not valid for any geometry of the plastic part. Finally there are some which analyze the part geometry in an internal way, through procedures closely linked to the CAD Modeler used for the part design.

In order to solve the problems presented above, a new method for the automatic design of the mold cooling system is presented. The method developed takes into account geometric, technical and functional parameters. The first stage of the algorithm recognizes in an automated way the discrete topology of the plastic part, and obtains the depth map of the part with the aim of detecting difficult cooling zones. Using this information, the algorithm automatically proposes the optimum design for cooling the part to suit its geometry. The algorithm recognizes large concavity areas of the part, slender details or internal turrets, which require baffle channels. Flat areas with no deep concavities are recognized and easily cooled by means of conventional horizontal straight channels. In this way a constant distance between the cooling channels and the surface of the part can be maintained, obtaining uniform conformal refrigeration but with reliable manufacturing methods, thus avoiding the high costs of additive manufacture. The algorithm verifies the possible interference of the cooling elements with other parts of the mold, ensuring its functionality. The dimensioning of the channels is performed by applying genetic optimization algorithms, thus guaranteeing the quality of the part. The method implemented presents as an additional advantage its independence from the modeler since it does not need internal information of the part, as the part is analyzed externally. Nor are CAE programs for later design validation required. As a final advantage, the algorithm is valid for any size of mold since it does not require Rapid Tooling techniques for its manufacture, allowing the use of traditional metallic materials by means of CNC procedures. To date there is no algorithm for the automatic design of the mold cooling system that resolves all the problems raised and assures the design efficiency for the industrial mold.

2. Background and related work

A large number of researchers and mold designers have focused their work on the cooling phase in injection molding, mainly improving the layout of the cooling channels as well as on the analysis and simulation of their new designs.

The first studies related to the design of cooling systems were carried out in the field of conventional systems [5-7]. Unfortunately all the designs presented had the disadvantage of a totally manual execution. In order to resolve this problem, several authors investigated the possible automation of the system design of conventional cooling channels in the injection mold. Many of the studies were based on the feature recognition method as an automated analysis of the topology of the plastic part. For the specific case of cooling systems, a cooling feature is defined as the surface fragment of the plastic part with information on its cooling. The cooling requirements for each feature are met using several cooling elements (cooling channels, bafflers, bubblers or helical baffles). Currently, the solid modeling of the part does not explicitly provide information about the features. For this reason we need recognition methods capable of extracting this implicit geometric information in the model in order to be used as input to later structured algorithms [8]. Li et al. [9] applied the Design Synthesis methodology together with the development of a new algorithm for the recognition of cooling features in the plastic part. In his study he decomposed the complex geometry of the plastic part into simpler parts. After its decomposition it recognizes the features, assigning to each of them the cooling subsystem best adapted to its geometry. Finally the set of cooling subsystems is synthesized in a single system for the whole part. The feature-based recognition method developed by Li allows the free geometry of the plastic part to be recognized as long as the surfaces forming it are similar to superquadric surfaces. Unfortunately, not all freeform surfaces can be represented as superquadric surfaces and therefore it is not a valid method for any plastic part. In a later study [10] it extends the automation of the conventional cooling system from the preliminary design phase to the layout phase of the channels. In this study preliminary design based on the recognition of features is considered as the basis, and then functional and manufacturing aspects are added. However, this study presents the same drawbacks as [9], based fundamentally on the process of recognition of features in the plastic part. The recognition of features from a part created in a CAD environment must be performed inside the modeler used to design it. It is also necessary to take into account the fact that the features interact. An interacting feature is the result of the intersection of multiple features. The difficulty in the recognition of these interacting features is mainly due to the destruction of the adjacency relations between features in contact. Li et al. [10] use fuzzy logic as an evaluation system for the different designs generated. The weighting ratios used by the evaluation system are selected by the mold maker based on their experience, which fails to meet the automation criteria of the design system, depending on the user. As a solution to the problems described above, Li et al. [11] developed a specific method for the conventional design of the cooling system based on the C-Space methodology, which allows the representation of a set of cooling designs without interfering with the rest of the components of the mold. This new method is an improvement on the heuristic method developed in [8], implementing a genetic algorithm integrated in the representation of the C-space in order to automatically generate the set of designs for the layouts. In a later paper Li et al. [12] improve on the C-Space method by allowing variations in geometry and topology of the design and incorporating user-defined constraints. However, the goal of their research is solely focused on the geometrical aspect of the cooling system, and technical parameters, related to the heat transfer between the plastic part and the mold, are not considered.

Most of the research work related to the design of cooling systems focuses on the design and analysis of conformal cooling channels. The design of conformal cooling channels in plastic injection has the advantage of greater uniformity in the cooling of the part since the cooling channels surround closely the cavity surface of the mold. The manufacture of molds cooled by conformal cooling channels, and more specifically of the core and cavity inserts, requires the use of rapid tooling techniques. In a pioneering study Sachs et al. [13] used 3D printing with stainless steel powder and a polymer binder to manufacture the mold cavity inserts incorporating a conformal channel design into an open ring-shaped part. However, the thermal properties of the mold material vary using conventional steel, this being a factor of influence not quantified in the behavior of the cooling system. Further research concerning new manufacturing methods for implementing conformal designs is found in [14, 15]. In the field of the implementation of conformal designs in prototype molds (rapid soft tools) Ferreira [16] made molds using a material composed of aluminum filled with epoxy resin. Unfortunately soft tooling molds are not useful for the manufacture of parts with a high level of surface quality for industrial use. In addition, the geometries of the channel layout are not fully adapted to the surface of the mold cavity in contact with the part. To solve these problems Saifullah [17] also uses bent copper tubes for the realization of the conformal cooling channels, but in mold manufactured by means of CNC, thus fulfilling the surface finishing requirement. However, the use of cooling channels by means of copper tubes can reduce the mold strength and its useful lifetime. The rapid tooling processes are capable of manufacturing the complex surfaces required by the cooling system, although most of these technologies are still at the laboratory development level and are not suitable for industrial use requirements. Recently Eiamsa [18] has used a new MIG / MAG melding torch manufacturing technique attached to a CNC machine as a hybrid system. In his study he built a layered mold designing the cooling by means of bubbler channels and then machining the surface. In the manufacture of cavities by means of conformal designs different research studies have been carried out aiming to improve the geometric design of conformal cooling channels with the help of CAD systems. Xu et al. [19] presented an analytical model for the dimensioning of the main technical parameters of the cooling system based on the decomposition of the mold surface into small sections called cooling zones, for which it creates an individual channel system. This configuration is again decomposed into smaller elements called cooling cells. A "design window", on which six design rules are applied, is created for each cell. Finally the individual results are grouped in order to construct the complete cooling system. Dimla et al. [20] proposes a method for the design and optimization of conformal cooling channels in cooling and heating processes using virtual prototypes. Quiao et al. [21] implemented a methodology for the optimization of the CAD design of the conformal channels, studying cooling by means of a sensitivity analysis based on the Boundary Elements Method and a hybrid type optimizer. The sensitivity analysis together with Boundary Element Coding showed good results, however they are not yet applicable to real cases of the industrial scope. Au et al. [22] used a uniform accuracy scaffolding architecture for the design of cooling channels. The results in the simulation analysis showed that this type of structure provided a more uniform cooling surface compared to conventional refrigeration designs and increased the mechanical strength of the mold cavities. Park et al. [23] used different types of layout (zigzag, parallel and spiral) for the conformal channels, applying analytical formulas and using CAE flow simulation to verify the results of the optimization process. Unfortunately [19-23] they required the interaction of the designer in some of the phases. In the field of automated design of the conformal cooling channels Au [24] proposed a methodology based on the use of geometric visibility algorithms to generate the automated design of the cooling channels and their application to complex surfaces in injection molds. In Au et al. [25] he continued his research by presenting an alternative design method consisting of a conformal cooling passageway with porous multi-connected characteristics, based on the principle of duality. In order to compensate the gradual increase in the temperature of the coolant from the input to the output pipes Au et al. [26] proposed a method of adjusting the distance between the conformal cooling channels and the surface of the cavities. With this new variable distance design, the heat is extracted more efficiently than by means of the existing conformal cooling channel designs. Wang et al. [27] proposed a new algorithm for the automated design of the conformal cooling circuit. The circuit proposed by the algorithm generates a surface adaptable to the surface of the part. Although the method was fully automated and only required a set of user parameters such as type of coolant, diameter of the cooling channels and cycle time, it also required an interactive optimization process performed by the designer, in order to adjust with enough precision the cooling channels using the cycle time value. Wang et al. [28] proposed a new algorithm for generating conformal cooling channels by means of a spiral layout. This configuration optimized the cooling system and reduced manufacturing costs. The conformal cooling channels provide uniform cooling of the part which reduces cooling time and increases the quality of the molded part, especially for long-sized products and free-form surfaces. The use of rapid prototyping techniques allows the production of cooling channels with very complex geometries in both mold cavities. Unfortunately the powdered metal materials used in 3D prototyping techniques are limited, and the functionality of the manufacturing process is not currently reliable for medium and large size molds as they are not able to meet industry requirements.

In addition to conventional and conformal systems, there are hybrid type systems for the design and manufacture of cooling channels. These methods take advantage of the manufacturing by means of CNC technologies allowing the use of traditional materials while maintaining a constant distance between the channel and the workpiece surface. There are two main hybrid cooling methods, the mechanized groove channel method, and the distribution of array of baffles structure. In the field of research of the design of the channel cooling systems by means of mechanized grooves Sun et al. [29] used a mechanized groove design with a U-shaped cooling channel surface. In their study the method is applied to large and complex free surface parts and compared to the design of conventional straight channels. Subsequently, Dang et al. [30] presented a systematic method for optimizing the design of grooved cooling channels, which reduces cooling time. In order to increase the computational efficiency of the algorithm it combines the analytical method with simulations, assessing the relationship between the thermal behavior of the mold and the parameters of the layout of the cooling channels. The cooling channel systems using a mechanized groove improve product quality by means of a higher uniformity in the cooling stage, and a lower cycle time, while a greater flexibility in the design of cooling channel layout is provided. However, high manufacturing costs prevent their use in large molds. Another hybrid method for the design of the cooling system is the design with structure of an array of baffles. It presents great advantages in its performance and low cost of manufacture. The array of baffles is characterized by being able to cool small regions of the core which are difficult to cool in medium and large size molds in parts with free form surfaces. Despite its many advantages, there are still few studies on how to optimize its distribution. In this regard, Park et al. [31] introduced the design of cooling channels by means of the array of baffles using a systematic method for the optimization of these channels. In his work he expressed, by means of explicit RMS equations, the relationship between the configuration of the cooling channels, the thickness of the part, the temperature distribution and the process parameters. The method proposed by Park improves the behavior of the cooling channels, facilitating the process of design optimization. However, this method still poses limitations since many of the requirements used to obtain the mathematical model are not real, which causes the final model to differ from the real model. In addition, the array of baffles in this study is considered as unique and covers the whole part. Usually the plastic parts have flat parts and concave parts, and it is not necessary to use baffles in reduced concavity areas.

To resolve these problems the paper presents a methodology for the automated design of the cooling system. In a first phase the algorithm recognizes the topology of the part in discrete format and obtains the depth map, detecting flat zones and changes in the geometry which make it difficult to cool. Using this information as a basis the algorithm proposes an optimal layout for the cooling system adapted to the part geometry. The algorithm employs horizontal straight channels in flat or low concave areas and uses the advantages of the design in the form of a baffle matrix for the concave areas, adapting the accuracy of the algorithm to the geometry to be manufactured. The method takes into account functional parameters by performing an automated analysis of the heat transfer in the mold, obtaining the limit distance from which the horizontal straight channels lose effectiveness, and guaranteeing a uniform cooling stage. In a second phase, the parameters of the cooling system such as channel diameter, channel gap, etc., are measured using genetic optimization algorithms. The result is the layout of the cooling system with the conformal system performance, maintaining a constant distance between the cooling channels and the surface of the part. At the same time the manufacture of the mold by means of CNC machines and traditional metallic materials is also possible, without the high costs of additive manufacturing. In addition, the algorithm performs an analysis of the interferences with other parts of the mold such as the ejection system. The method does not need a subsequent CAE analysis since it takes into account functional and technical parameters related to heat transfer in its design, thus ensuring its functionality. The algorithm is independent of the modeler used to design the part since it performs a procedure of surface recognition. Moreover, the design is achieved by means of an external process which can be implemented in any CAD system. The data obtained can be used additionally in later applications including the automated design of the injection mold.

3. Methodology

3.1. Discrete model of the plastic part

The proposed algorithm performs a previous processing of the part $\mathcal{D} \in \mathbb{R}^3$ in order to obtain the discrete three-dimensional mesh $\mathcal{D}' \in \mathbb{R}^3$, consisting of a set of triangular facets $F_i \in \mathcal{D}'_f$, being nx3 the range of the array $\mathcal{D}'_f$ and a set of nodes $P_{ij} = \{X_{ij}, Y_{ij}, Z_{ij}\} \in \mathcal{D}'_n$, being the array $\mathcal{D}'_n$ of range 3·nx3 Eq.(1). The value of n coincides with the total number of triangular facets F_i that makes up the mesh $\mathcal{D}'$.

$$\forall\ \mathcal{D} \in \mathbb{R}^3 \rightarrow \mathcal{D}' \in \mathcal{M}_{1x2}\ (\mathbb{R}) \rightarrow \mathcal{D}' = \{\mathcal{D}'_f \quad \mathcal{D}'_n\}$$

$$\mathcal{D}'_f \in \mathcal{M}_{\mathrm{n}xm}\ (\mathbb{R}^3) \quad ; \quad \mathcal{D}'_n \in \mathcal{M}_{3\cdot \mathrm{n}xm}\ (\mathbb{R}^3) \tag{1}$$

Where m is the number of nodes per facet $F_i \in \mathcal{D}'_f$. The proposed method uses triangulate facets with the value of the parameter m being equal to 3, being able to extend the scope of the method to facets with any other flat polygonal geometry. Fig. 1 shows the continuous CAD model $\mathcal{D}$ of the plastic part to be analyzed together with the discrete mesh $\mathcal{D}'$ obtained after the pre-processing phase. Fig 2 shows a detail of a triangular facet $F_{ij} = \{P_{i1}, P_{i2}, P_{i3}\} \in \mathcal{D}'_f$, and the nodes $P_{ij} \in \mathcal{D}'_n$ that compose it.

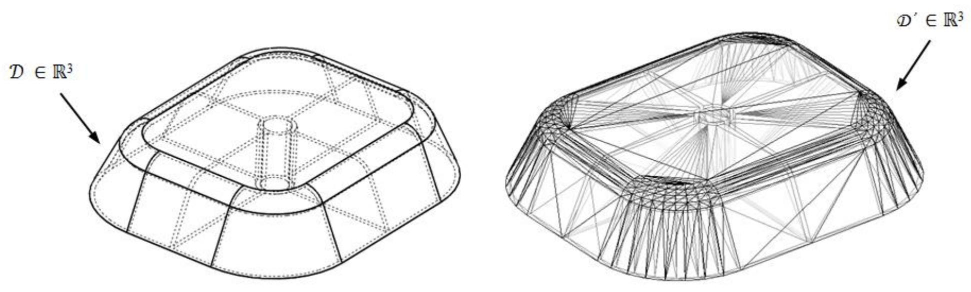

Fig. 1.- CAD model $\mathcal{D}$ and discrete geometry $\mathcal{D}'$ of the plastic part.

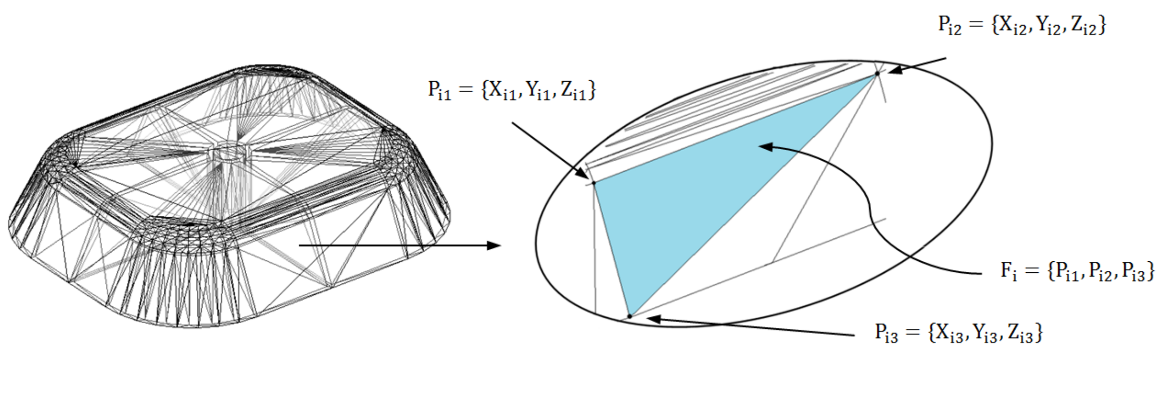

Fig 2.- Detail of a triangular facet F_i of the mesh $\mathcal{D}'$ and the nodes P_{i1}, P_{i2}, P_{i3}.

3.2. Obtaining the depth map of the mesh 𝒟'

The objective of this phase of the algorithm is to determine the depth map $[\tau_{cavity}, \ \tau_{core}] \in \mathbb{R}^3$ of the surfaces belonging to 𝒟' to be molded by the cavity and core plates respectively. The depth map provides information about the surface topology of the 𝒟' mesh. This information is of great help in the automated design of the cooling system since it allows identification of those regions belonging to 𝒟' which, due to their depth, require the use of additional cooling elements such as baffles.

The first step to obtaining the depth map is to locate the set of surfaces belonging to $\mathcal{D} \in \mathbb{R}^3$ to be molded by means of the core and cavity plates. For this, the algorithm developed is based on the results obtained in the demoldability analysis [2] applied to the mesh $\mathcal{D}' \in \mathbb{R}^3$. Thus the mesh $\mathcal{D}_f' \in \mathbb{R}^3$ is segmented into two regions $\{\Omega_{f1} \ \cup \ \xi_{f2}\}$ Eq. (2) sorted by their demoldability with respect to the main parting direction $\overrightarrow{D_z}$.

In Fig 3 the result of the demoldability analysis [2] applied to the mesh $\mathcal{D}' \in \mathbb{R}^3$ is shown. The zones to be molded by means of the cavity plate have been represented in green and the zones to be molded by means of the core plate in blue, where $\overrightarrow{D_z}$ is the parting direction for 𝒟.

$$\forall \mathcal{D}_f' \ \exists \{ \Omega_{f1} \ \cup \ \xi_{f2} \}$$

$$f_1+f_2=f \tag{2}$$

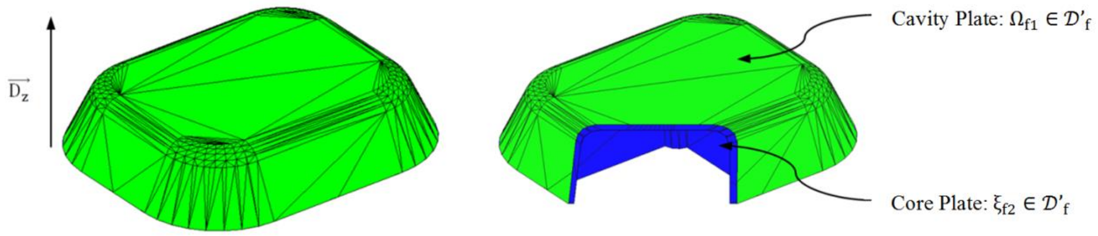

Fig.3.- Demolding analysis of part 𝒟'.

Similarly, the nodes $\mathcal{D}_n' \in \mathbb{R}^3$ belonging to the set of facets $\Omega_{f1} \in \mathbb{R}^3$ are grouped in the array $\Omega_{n1} \in \mathbb{R}^3$ Eq.(3), and the nodes belonging to the set of facets $\xi_{f2} \in \mathbb{R}^3$ to be molded by means of the core plate, in the array $\xi_{n2} \in \mathbb{R}^3$ (Fig 4).

$$\forall \mathcal{D}_n' \ \exists \{ \Omega_{n1} \ \cup \ \xi_{n2} \}$$

$$n_1+n_2=n \tag{3}$$

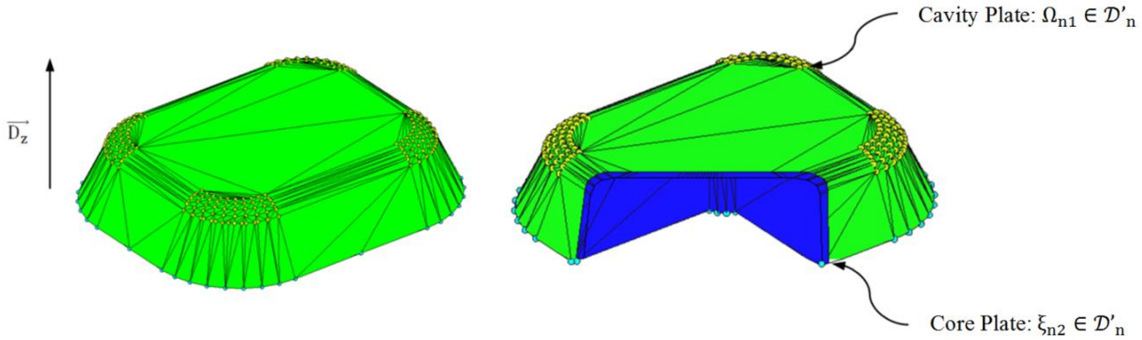

Fig. 4.- Demoldability analysis of part 𝒟'. The nodes belonging to the arrays Ω_{n1}, ξ_{n2} are highlighted.

After segmenting the set of facets $\mathcal{D}'_f \in \mathbb{R}^3$ according to its demoldability by means of the meshes Ω_{f1} y ξ_{f2}, the depth map is obtained. First, the Bounding Box of the mesh $\mathcal{D}' \in \mathbb{R}^3$ is generated from its principal dimensions *l*, *w* and *h* in the coordinate axes X, Y, Z respectively (see Fig 5a and Fig 5b). Using the dimensions *w* (width) and *l* (length) of the Bounding Box, two two-dimensional nodal meshes of precision ε equal to the dimensional value of the minimum thickness of the plastic part $\mathcal{D} \in \mathbb{R}^3$ are created. The nodal mesh corresponding to the region Ω_{f1}, which can be molded by means of the cavity plate, is stored in the array $\Theta_{t_{cavity}}$ and the nodal mesh corresponding to the region ξ_{f2}, which can be molded by means of the core plate, is stored in the array $\Theta_{t_{core}}$ (Fig 5a and Fig 5b) Eq.(4).

$$[\Theta_{t_{cavity}} \quad \Theta_{t_{core}}] \in \mathcal{M}_{\frac{l}{\varepsilon} x \frac{w}{\varepsilon}} (\mathbb{R}) \tag{4}$$

Both nodal meshes $\Theta_{t_{cavity}}$, $\Theta_{t_{core}}$ are composed of a set of nodes $\theta_{t_{cavity}}(i,j) \in \mathbb{R}^3$ and $\theta_{t_{core}}(i,j) \in \mathbb{R}^3$ with coordinates $[\theta_{t_{cavity}}(i,j)_x \quad \theta_{t_{cavity}}(i,j)_y \quad \theta_{t_{cavity}}(i,j)_z]$ and $[\theta_{t_{core}}(i,j)_x \quad \theta_{t_{core}}(i,j)_y \quad \theta_{t_{core}}(i,j)_z]$ Eq.(5). The nodes $\theta_{t_{cavity}}(i,j) \in \mathbb{R}^3$ and $\theta_{t_{core}}(i,j) \in \mathbb{R}^3$ share coordinates in the X, Y axes, differing in the value of the coordinate in the Z axis $\theta_{t_{cavity}}(i,j)_z$ y $\theta_{t_{core}}(i,j)_z$ (See Fig 5a and 5b).

$$\forall \begin{bmatrix} i \\ j \end{bmatrix} \in \begin{Bmatrix} 1, \dots, i, \dots, \frac{l}{\varepsilon} \\ 1, \dots, j, \dots, \frac{w}{\varepsilon} \end{Bmatrix} \exists \begin{bmatrix} \theta_{t_{cavity}}(i,j) = [\theta_{t_{cavity}}(i,j)_x \quad \theta_{t_{cavity}}(i,j)_y \quad \theta_{t_{cavity}}(i,j)_z] \in \mathbb{R}^3 \\ \theta_{t_{core}}(i,j) = [\theta_{t_{core}}(i,j)_x \quad \theta_{t_{core}}(i,j)_y \quad \theta_{t_{core}}(i,j)_z] \in \mathbb{R}^3 \end{bmatrix} \mid \begin{bmatrix} \theta_{t_{cavity}}(i,j)_x = \theta_{t_{core}}(i,j)_x \\ \theta_{t_{cavity}}(i,j)_y = \theta_{t_{core}}(i,j)_y \\ \theta_{t_{cavity}}(i,j)_z \neq \theta_{t_{core}}(i,j)_z \end{bmatrix} \tag{5}$$

For the set of nodes $\Theta_{t_{cavity}} \in \mathbb{R}^3$ the value of $\theta_{t_{cavity}}(i,j)_z$ is constant for each node $\theta_{t_{cavity}}(i,j) \in \mathbb{R}^3$ and equal to the coordinate in the direction $\overrightarrow{D_z}$ of the node with the highest dimension $\Omega_{n1}(i,j)_{zmax}$ belonging to the mesh $\Omega_{n1} \in \mathcal{D}'_n$(See Fig 5a) Eq.(6). In the same way, for the set of nodes $\Theta_{t_{core}} \in \mathbb{R}^3$, the value of $\theta_{t_{core}}(i,j)_z$ is constant for each node $\theta_{t_{core}}(i,j)$ and equal to the coordinate in the direction $\overrightarrow{D_z}$ of the node with the lowest dimension $\xi_{n2}(i,j)_{zmin}$, belonging to the mesh $\xi_{n2} \in \mathcal{D}'_n$ (See Fig 5b).

$$\begin{bmatrix} \theta_{t_{cavity}}(i,j)_z = \Omega_n(i,j)_{zmax} = Cons \\ \theta_{t_{core}}(i,j)_z = \xi_n(i,j)_{zmin} = Cons \end{bmatrix} \tag{6}$$

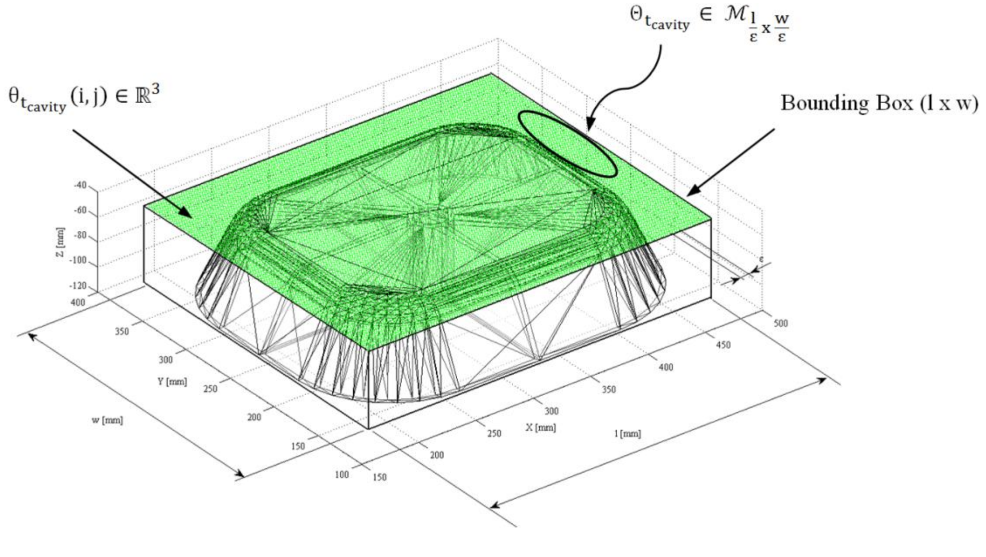

Fig. 5a.- Location of the Bounding Box and measures w and l on the XY plane in cavity plate analysis.

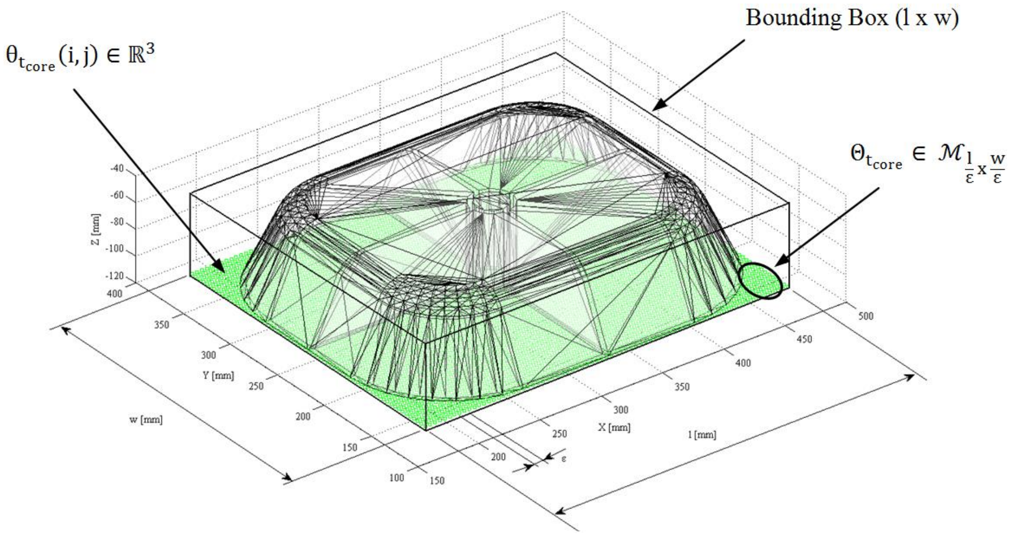

Fig. 5b.- Location of the Bounding Box and measures w and l on the XY plane in core plate analysis.

Next, for each node $\theta_{t_{cavity}}(i,j) \in \Theta_{t_{cavity}} \in \mathbb{R}^3$and for each node $\theta_{t_{core}}(i,j) \in \Theta_{t_{core}} \in \mathbb{R}^3$ two sets of lines $\mathcal{R}_{t_{cavity}}$ and $\mathcal{R}_{t_{core}}$ are generated Eq.(7). The lines have as starting point each node $\theta_{t_{cavity}}(i,j) \in \mathbb{R}^3$ and $\theta_{t_{core}}(i,j) \in \mathbb{R}^3$, their directing vector being coincident with the parting direction $\overrightarrow{D_z}$. The intersection of the lines $\mathcal{R}_{t_{cavity}}$ and $\mathcal{R}_{t_{core}}$ with the sets of facets $\Omega_{f1} \in \mathbb{R}^3$ and $\xi_{f2} \in \mathbb{R}^3$ generates new nodes $\lambda_{t_{cavity}}(i,j) \in \mathbb{R}^3$ and $\lambda_{t_{core}}(i,j) \in \mathbb{R}^3$ that are contained in $\Omega_{f1} \in \mathbb{R}^3$ and $\xi_{f2} \in \mathbb{R}^3$ respectively Eqs.(8)-(9). The nodes $\lambda_{t_{cavity}}(i,j)$ are shown in Fig 6a and the nodes $\lambda_{t_{core}}(i,j) \in \mathbb{R}^3$ are shown in Fig 6b.

$$\left[\mathcal{R}_{t_{cavity}} \quad \mathcal{R}_{t_{core}}\right] \in \mathcal{M}_{\frac{l}{\varepsilon} x \frac{w}{\varepsilon}}(\mathbb{R}) \rightarrow \left[\mathcal{R}_{t_{cavity}} \quad \mathcal{R}_{t_{core}}\right] := \left[r_{t_{cavity}}(i,j)_{\frac{l}{\varepsilon} x \frac{w}{\varepsilon}} \quad r_{t_{core}}(i,j)_{\frac{l}{\varepsilon} x \frac{w}{\varepsilon}}\right] \tag{7}$$

$$\forall\, \lambda_{t_{cavity}}(i,j)\ \exists\ r_{t_{cavity}}(i,j) = \begin{Bmatrix} \text{Origin: } \left[\theta_{t_{cavity}}(i,j)_X \quad \theta_{t_{cavity}}(i,j)_Y \quad \theta_{t_{cavity}}(i,j)_Z\right] \\ \text{Direction: } [0\ 0\ 1] \end{Bmatrix} \in \mathbb{R}^2$$

$$\forall\, \lambda_{t_{core}}(i,j)\ \exists\ r_{t_{core}}(i,j) = \begin{Bmatrix} \text{Origin: } \left[\theta_{t_{core}}(i,j)_X \quad \theta_{t_{core}}(i,j)_Y \quad \theta_{t_{core}}(i,j)_Z\right] \\ \text{Direction: } [0\ 0\ 1] \end{Bmatrix} \in \mathbb{R}^2 \tag{8}$$

$$\forall\, r_{t_{cavity}}(i,j) \mid \{ r_{t_{cavity}}(i,j) \cap \Omega_f\} \neq \emptyset \rightarrow \lambda_{t_{cavity}}(i,j) \in \mathbb{R}^3$$

$$\forall\, r_{t_{core}}(i,j) \mid \{ r_{t_{core}}(i,j) \cap \xi_f\} \neq \emptyset \rightarrow \lambda_{t_{core}}(i,j) \in \mathbb{R}^3 \tag{9}$$

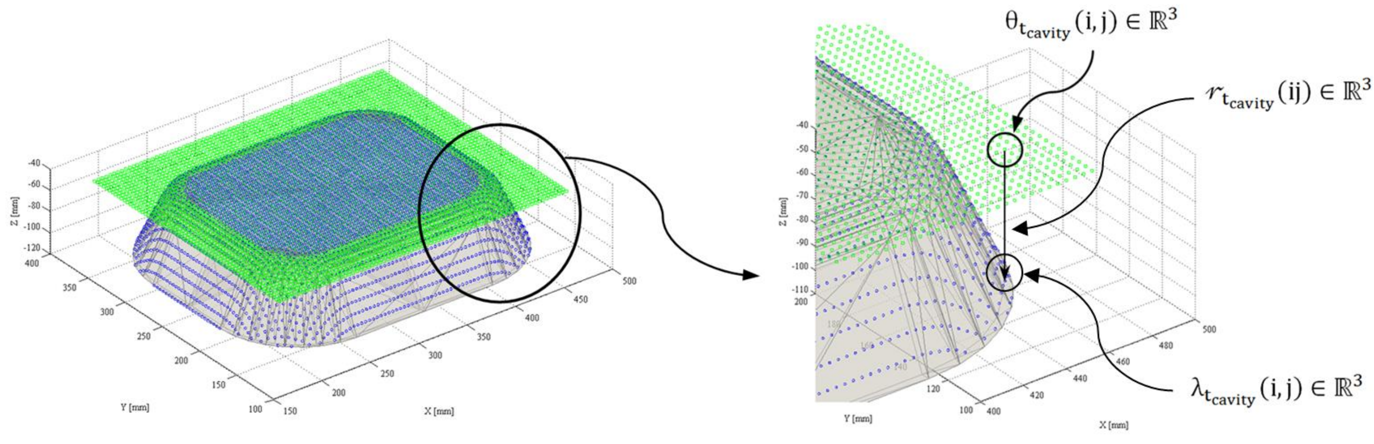

Fig. 6a.- Obtaining intersection points between an individual line $r_{t_{cavity}}(ij)$ and the part $\mathcal{D}' \in \mathbb{R}^3$.

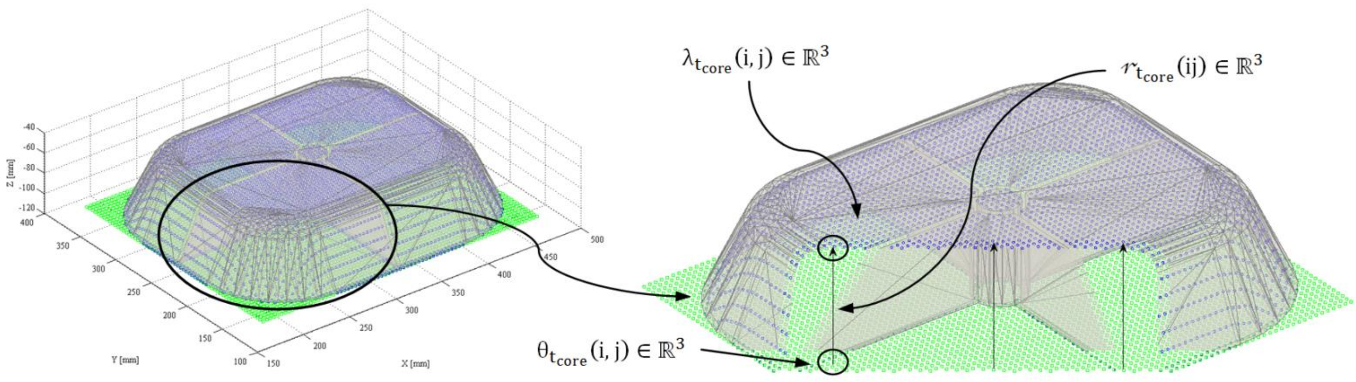

Fig. 6b.- Obtaining intersection points between an individual line $r_{t_{core}}(ij)$ and the part $\mathcal{D}' \in \mathbb{R}^3$.

The map of depths $[\tau_{cavity}, \ \tau_{core}] \in \mathbb{R}^3$ for the regions $\Omega_{f1} \in \mathbb{R}^3$ y $\xi_{f2} \in \mathbb{R}^3$ is obtained from the distances $\tau_{cavity}(i,j)$ and $\tau_{core}(i,j)$ between each node $\theta_{t_{cavity}}(i,j) \in \mathbb{R}^3$, $\theta_{t_{core}}(i,j) \in \mathbb{R}^3$ and its analogue node $\lambda_{t_{cavity}}(i,j) \in \mathbb{R}^3$ and $\lambda_{t_{core}}(i,j) \in \mathbb{R}^3$ Eq.(10). The depth map $\tau_{cavity} \in \mathbb{R}^3$ for the $\mathcal{D}'$ mesh is shown in Fig 7a and the depth map $\tau_{core} \in \mathbb{R}^3$ for the $\mathcal{D}'$ mesh is shown in Fig 7b. The depth parameters $\tau_{cavity}(i,j) \in \mathbb{R}^3$ and $\tau_{core}(i,j) \in \mathbb{R}^3$ are indicated by means of a color coding. The graduated bars on the right in Figs. 7a and 7b indicate the dimensional value in millimeters of the depth parameters $\tau_{cavity}(i,j)$ and $\tau_{core}(i,j)$, respectively.

$$\forall\, \lambda_{t_{cavity}}(i,j)\ \exists\ \tau_{cavity}(i,j) \in \mathbb{R} \mid \tau_{cavity}(i,j) = \left|\theta_{t_{cavity}}(i,j) \quad \lambda_{t_{cavity}}(i,j)\right|$$

$$\forall\, \lambda_{t_{core}}(i,j)\ \exists\ \tau_{core}(i,j) \in \mathbb{R} \mid \tau_{core}(i,j) = \left|\theta_{t_{core}}(i,j) \quad \lambda_{t_{core}}(i,j)\right| \qquad (10)$$

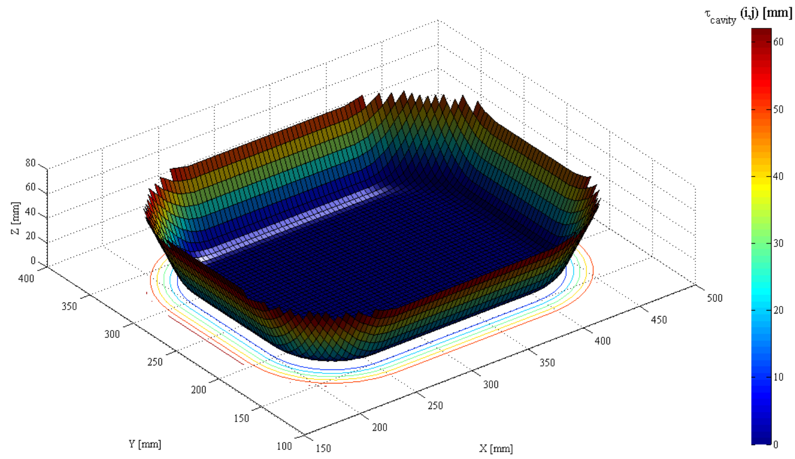

Fig. 7a.- Depth map τ_{cavity} for the mesh $\mathcal{D}'$.

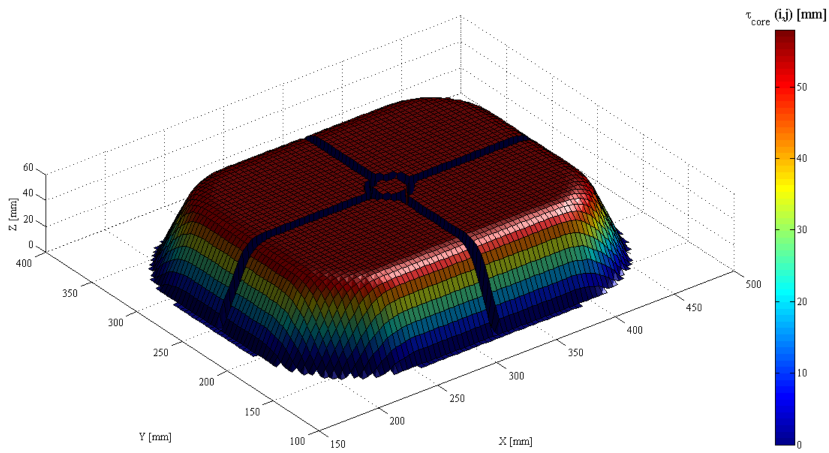

Fig. 7b.- Depth map τ_{core} for the mesh $\mathcal{D}'$.

3.3. Dimensioning of the geometric and technical parameters of the cooling system.

This section describes the dimensioning process of the geometric and technical parameters that define the cooling system for the plastic part. The dimensioning of the cooling system for the plastic part is performed by genetic optimization algorithms. The use of genetic algorithms allows the cooling system to adapt to a series of requirements or boundary conditions that the design must meet, obtaining the optimum result.

First, the technical and geometric variables of the refrigeration system that the genetic algorithm has to optimize are determined (Table 1).

Nomenclature	Units	Description	Notation on the optimization problem	Constraints
$\overline{T_m}$	ºC	Mold cavity surface temperature	x(1)	$23 \leq x(1) \leq T_{ejec}$
T_c	ºC	Coolant temperature	x(2)	$10 \leq x(2) \leq 99$
L_b	mm	Distance between cooling channels	x(3)	$10 + 14 \leq x(3)$
$D_{baffles}$	mm	Diameter of cooling channels	x(4)	$8 \leq x(4) \leq 14$

Table 1.- Variables of the technical optimization problem.

The value of the variable L_p [mm], corresponding to the distance between the baffle and the plastic part, is assumed constant and equal to 10 mm based on criteria of industrial experience. The magnitude of the other characteristic parameters of the polymer and the mold material are: ρ_p, c_p, δ_s, h, T_{melt}, T_{eject} and α_s. They are established according the manufacturers´ recommendations.

The optimization process using genetic algorithms requires the definition of fitness functions, to be minimized or maximized according to the requirements of an optimum design of the cooling system, and constraint parameters, to be satisfied in terms of optimization variables. For the proposed physical model, the optimization problem can be defined as shown in Table 2.

Genetic Algorithm Options Structure	Defined Set-up	Description
Population	Double vector	Initial population from which the evolutionary cycle begins. "Double Vector" method since the variables are of double and decimal type.
Scaling Function	Fitness Rank	A scaling function increases the differentiation between the optimal ones, reducing the probabilities of generating individuals with less aptitude in subsequent generations.
Selection	Uniform Stochastic	Local search around promising solutions without losing the randomness component needed to explore other solutions in the search domain.
Reproduction	Two Points	Generation of the children corresponding to each new generation, based on the arithmetic mean of two randomly selected parents of the population.
Mutation	2%	Fraction of the individuals of the mutated population, whose value is replaced by another random value chosen from the population range.
Crossover factor	80%	Crossover factor specifying the fraction of individuals of the next generation that is susceptible to cross-over.
Migration	Direction: Forward Migration Interval: 20 Migration factor: 0.3	Forward traslation of individuals of the population between regions of the domain. At each migration interval the best individuals of one generation (selected via the migration factor) replace the worst of another region.

Table 2.- Definition of the technical optimization problem.

The constraints have been set according to the limit values that the variables of the optimization problem can take. It is assumed that the coolant temperature will not exceed or fall below the limit values of the vacutherm coolant temperature controller [40]. Mold cavity surface temperature will not exceed the part ejection temperature or be lower than the ambient temperature (assumed for the standard operation of an injection mold). The spacing L_b between baffles or cooling channels will not be less than 10 mm to avoid compromising the structural safety of the mold. And finally, the dimension of the diameters of the cooling channels $D_{baffles}$ will be limited according to the experience and the standardization criteria of the industry.

In order to complete the multi-objective optimization problem, it is necessary to introduce the set of objective functions to be optimized. The first objective function is intended to minimize the difference between mold cavity surface temperature x(1) (variable of the optimization problem) and its resulting value according to the proposed physical model Eqs.(11)-(12).

$$\text{Fitness Function}_1 : \text{Min}\{\sigma(x(1), \overline{T_m})\} \tag{11}$$

Where $\sigma(x(1), \overline{T_m})$ represents the standard deviation between the variable x(1) and mold cavity surface of the proposed physical model.

$$\text{Fitness Function}_1 : \text{Min}\left\{\sigma\left(x(1), \left[x(2) + \frac{\rho_p \cdot c_p \cdot T_h \cdot (2 \cdot \delta_s \cdot x(3) + h \cdot \pi \cdot x(4) \cdot L_p) \cdot (T_{melt} - T_{eject})}{h \cdot \pi \cdot x(4) \cdot \delta_s \cdot t_{cycle}}\right]\right)\right\} \tag{12}$$

Secondly, in order to ensure the structural integrity of the injection mold and reduce the costs derived from the machining of the mold, it is proposed to maximize the distance between baffles Eq.(13).

$$\text{Fitness Function}_2 : \text{Max}\{x(3)\} \tag{13}$$

Thirdly, in order to ensure the structural integrity of the injection mold it is proposed to minimize the diameters of the cooling channels Eq.(14).

$$\text{Fitness Function}_3 : \text{Min}\{x(4)\} \tag{14}$$

Finally, minimizing the cycle time is proposed in order to improve the efficiency and lower the costs of the manufacturing process Eq.(15). It is important to note that minimizing the cycle time involves reducing the mold cavity surface temperature. Occasionally this causes increases in the residual stress of the part, so some constraints of the variables of the optimization problem are established to avoid this unfavorable situation. Finally, the results obtained will be tested using numerical software to check the validity of the physical model.

$$\text{Fitness Function}_4 : \text{Min}\{t_{cycle}\} = \text{Min}\left\{\frac{T_h^2}{\pi^2 \cdot \alpha_s} \cdot \text{Ln}\left(\frac{4}{\pi} \cdot \frac{T_{melt} - x(1)}{T_{eject} - x(1)}\right)\right\} \tag{15}$$

3.4. Locating regions of mesh 𝒟' to be cooled by means of baffles or horizontal straight channels

Based on the geometric data of the depth map $[\tau_{cavity}, \ \tau_{core}] \in \mathbb{R}^3$, the proposed algorithm determines the regions belonging to 𝒟' that can be cooled using horizontal straight channels and the regions belonging to 𝒟' which, due to their depth and geometry, require more specific cooling systems such as the use of baffles.

3.4.1. Location of regions of the 𝒟' mesh cooled by means of baffles

This section determines the plastic part regions that require the use of auxiliary cooling elements such as baffles. The location of the main cooling channels, and especially the baffles, depends basically on the geometrical characteristics of the plastic part. Flat, slim and shallow parts can be cooled using a conventional channels system without the need for baffles. However, pieces with large concavities, internal turrets, housings, etc. require the application of baffles to improve the cooling process and to bring the coolant to concave regions where the perforated rectilinear channels lose their functionality. The operating structure of a baffle system is shown in Fig 8.

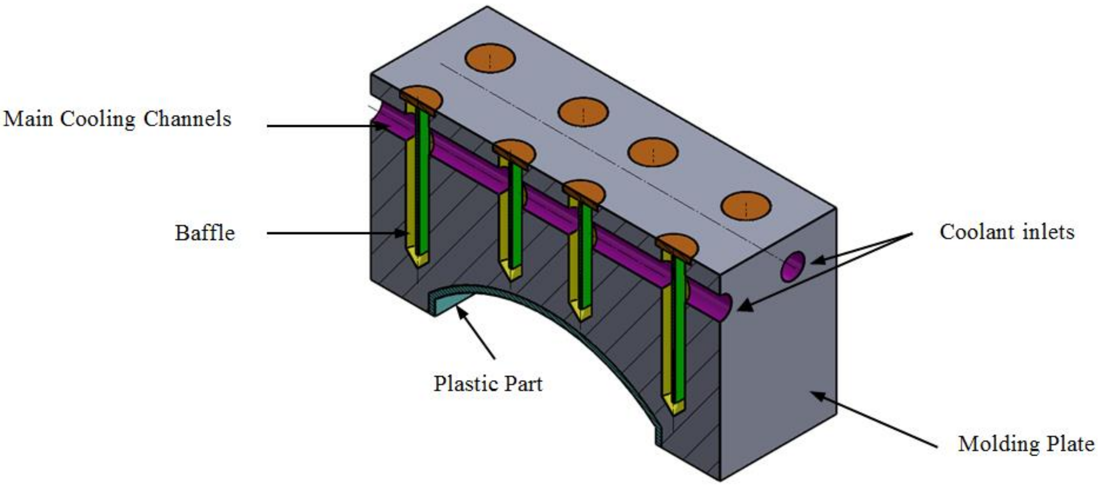

Fig. 8.- Cooling system by means of baffles.

The purpose of this section is to determine the magnitude of the limit range distance from which perforated straight channels lose effectiveness and are not capable of cooling deep regions of the plastic part. To do this, the heat flow provided by the melt plastic flow is estimated according to the Fourier Law as Eq.(16).

$$\dot{Q}_{inj} = \frac{\left(c_p \cdot (T_{melt} - T_{eject}) + i_m\right) \cdot \rho_p \cdot \upsilon_p}{t_{cycle}} \tag{16}$$

Where $\dot{Q}_{inj}$ [W] represents the heat flow per unit time given by the melt plastic to the mold, i_m [J/kg] the latent heat of fusion of the polymer, and υ_p [mm^3] the volume of injected polymer. Since the present model studies the cavity and core plate independently, the heat transferred by the melt plastic flow is evenly distributed according to the region of the part demolded by means of cavity and core plate, respectively Eqs.(17)-(18).

$$\dot{Q}_{inj} = \dot{Q}_{inj_{cavity}} + \dot{Q}_{inj_{core}} \tag{17}$$

Where.

$$\dot{Q}_{inj_{cavity}} = \dot{Q}_{inj} \cdot \frac{A_{cavity}}{A_{cavity} + A_{core}} \quad ; \quad \dot{Q}_{inj_{core}} = \dot{Q}_{inj} \cdot \frac{A_{core}}{A_{cavity} + A_{core}} \tag{18}$$

A_{cavity} [mm^2] is the area of the region of the part that is molded by means of a cavity plate and A_{core} [mm^2] the area of the region of the part that is molded by means of core plate. After evaluating the heat flow transferred by the melt plastic to the cavity plate and the core plate respectively, and according to the Fourier law, the safety distances $L_{S_{cavity}}$ and $L_{S_{core}}$ from which the perforated rectilinear channels lose effectiveness are set as Eq.(19).

$$L_{S_{cavity}} = \frac{A_{cavity} \cdot \delta_s}{\dot{Q}_{inj_{cav}}} \cdot \left(\overline{T_m} - T_{C_{min}}\right) \quad ; \quad L_{S_{core}} = \frac{A_{core} \cdot \delta_s}{\dot{Q}_{inj_{cor}}} \cdot \left(\overline{T_m} - T_{C_{min}}\right) \tag{19}$$

Where $T_{C_{min}}$ [ºC] represents the minimum operating temperature of the coolant, i.e. the minimum temperature from which the fluid loses its cooling properties. The magnitude of this parameter is 10 °C according to the limit values of the vacutherm coolant temperature controller (see Table 1, 2) [34].

Finally, based on the depth map of the mesh $\mathcal{D}$' ($\tau_{cavity} \in \mathbb{R}^3$ y $\tau_{core} \in \mathbb{R}^3$) (Figs 7a and 7b) the nodes $\lambda_{t_{cavity}}(i,j) \in \mathbb{R}^3$, $\lambda_{t_{core}}(i,j) \in \mathbb{R}^3$ whose depth $\tau_{cavity}(i,j)$, $\tau_{core}(i,j)$ is greater than the safety distances $L_{S_{cavity}}$ y $L_{S_{core}}$ are located Eq.(20). Thus, if a node $\lambda_{t_{cavity}}(i,j) \in \mathbb{R}^3$ meets the condition of having a depth $\tau_{cavity}(i,j) \in \mathbb{R}^3$ greater than $L_{S_{cavity}}$ it is stored in the array $\beta_{cavity}(i,j) \in \mathbb{R}^3$. Similarly, if a node $\lambda_{t_{core}}(i,j) \in \mathbb{R}^3$ meets the condition of having a depth $\tau_{core}(i,j) \in \mathbb{R}^3$ greater than $L_{S_{core}}$ it is stored in array $\beta_{core}(i,j) \in \mathbb{R}^3$.

$$\forall\, \lambda_{t_{cavity}}(i,j) \in \mathbb{R}^3 \mid \tau_{cavity}(i,j) \geq L_{S_{cavity}} \rightarrow \lambda_{t_{cavity}}(i,j) \in \beta_{caviy}(i,j) \in \mathbb{R}^3 \tag{20}$$

$$\forall\ \lambda_{t_{core}}(i,j) \in \mathbb{R}^3 \mid \tau_{core}(i,j) \geq L_{S_{core}} \rightarrow \lambda_{t_{core}}(i,j) \in \beta_{core}(i,j) \in \mathbb{R}^3$$

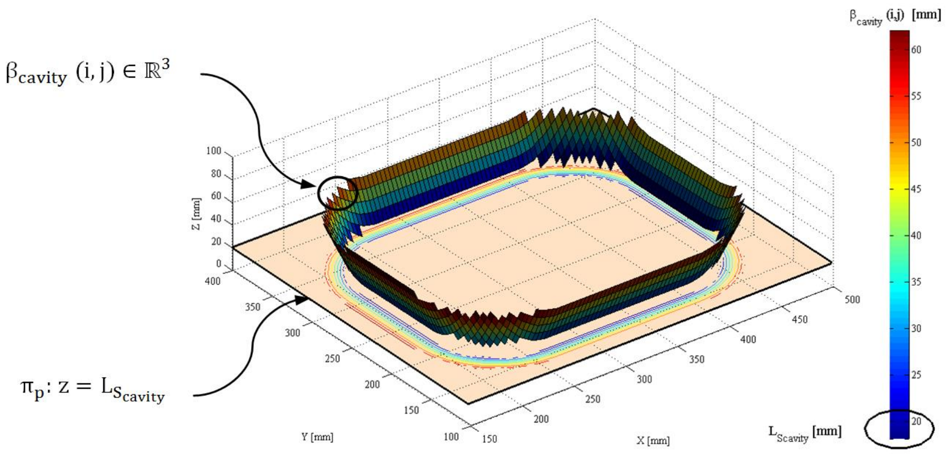

Fig. 9a.- Obtaining nodes $\beta_{cavity}(i,j)$ from the depth map τ_{cavity} of the plastic part.

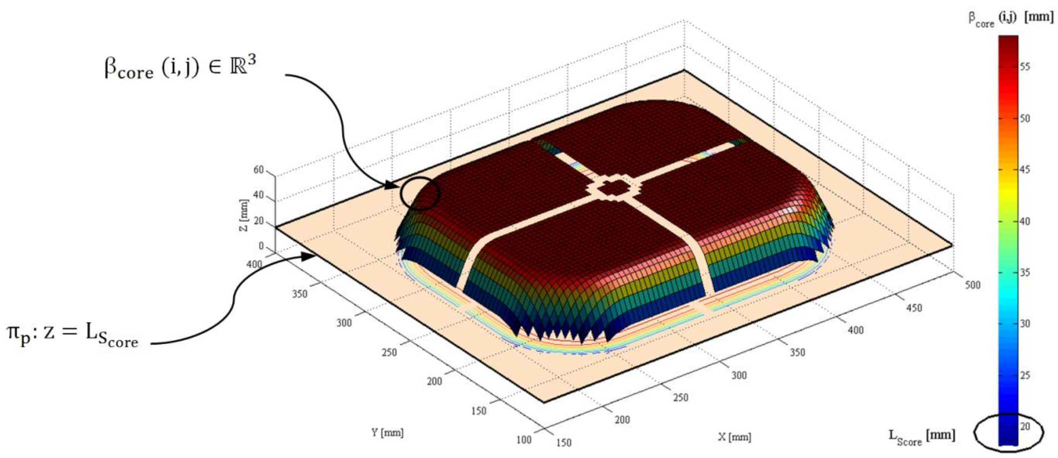

Fig. 9b.- Obtaining nodes $\beta_{core}(i,j)$ from the depth map τ_{core} of the plastic part.

Fig. 9a shows the depth map $\tau_{cavity}(i,j) \in \mathbb{R}^3$ for the surfaces $\Omega_{f1} \in \mathbb{R}^3$. The map τ_{cavity} represents the depth of each node $\lambda_{t_{cavity}}(i,j)$ of the mesh $\Omega_{f1} \in \mathbb{R}^3$ by means of a color coding. The graduated bar on the right indicates the values $\tau_{cavity}(i,j)$ in millimeters for each node $\lambda_{t_{cavity}}(i,j)$. The locus of the parameter $L_{S_{cavity}}$ is represented by the plane $\pi_p: z = L_{S_{cavity}}$. For the mesh $\Omega_{f1} \in \mathbb{R}^3$of Fig. 9a the value $L_{S_{cavity}}$is 20 mm. The regions of Ω_{f1} whose depth $\tau_{cavity}(i,j)$ is greater than 20 mm are stored in the array $\beta_{cavity}(i,j) \in \mathbb{R}^3$, requiring the use of baffles for the design of their cooling system. Fig 9b indicates the depth map $\tau_{core}(i,j) \in \mathbb{R}^3$for the mesh $\xi_{f2} \in \mathbb{R}^3$. The locus of the parameter $L_{S_{core}}$ is represented by the plane $\pi_p: z = L_{S_{core}}$. In Fig 10b the location of nodes $\beta_{core}(i,j) \in \mathbb{R}^3$whose depth is greater than $L_{S_{core}}$, and therefore require the use of baffles for the design of their cooling system, has been indicated.

3.4.2. Location of regions of 𝒟' mesh cooled by a straight horizontal channel system

On the other hand, this section determines the plastic part regions that do not require the use of auxiliary cooling elements such as baffles. For those regions of the plastic part whose depth $\tau_{cavity}(i,j) \in \mathbb{R}^3$ and $\tau_{core}(i,j) \in \mathbb{R}^3$ do not exceed the safety distance $L_{S_{cavity}}$ y $L_{S_{core}}$ respectively, the proposed methodology is adapted using a traditional solution of perforated straight channels. Thus, if a node $\theta_{t_{cavity}}(i,j)$ meets the condition of having a depth $\tau_{cavity}(i,j) \in \mathbb{R}^3$ less than $L_{S_{cavity}}$, then it is stored in the array $\omega_{cavity}(i,j) \in \mathbb{R}^3$. Similarly, if a node $\theta_{t_{core}}(i,j)$ satisfies the condition of having a depth $\tau_{core}(i,j) \in \mathbb{R}^3$ greater than $L_{S_{core}}$, then is stored in array $\omega_{core}(i,j) \in \mathbb{R}^3$. Fig 10a shows the nodes $\omega_{cavity}(i,j) \in \mathbb{R}^3$ by means of the depth map $\tau_{cavity}(i,j) \in \mathbb{R}^3$.

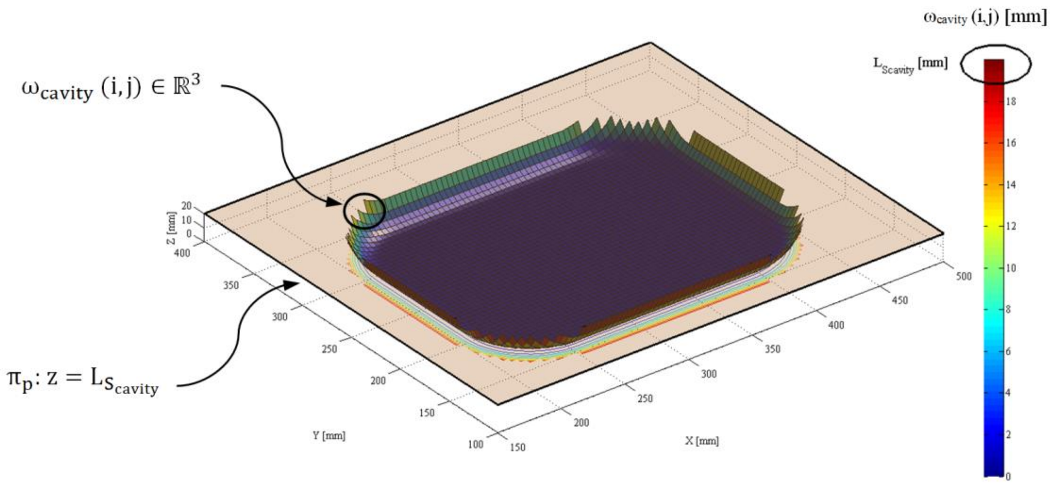

Fig. 10a.- Obtaining nodes $\omega_{cavity}(i,j)$ from the depth map τ_{cavity} of the plastic part.

Fig 10b shows the nodes $\omega_{core}(i,j) \in \mathbb{R}^3$ by means of the depth map $\tau_{core}(i,j) \in \mathbb{R}^3$.

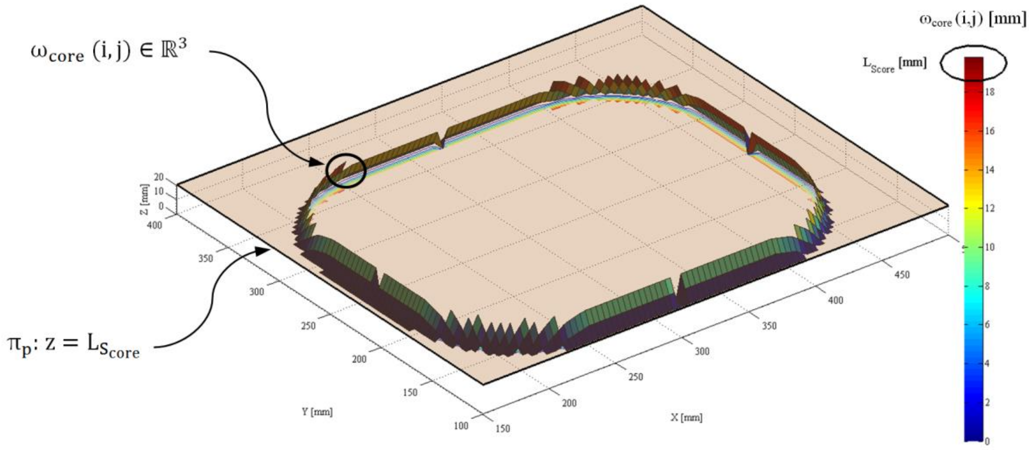

Fig. 10b.- Obtaining nodes $\omega_{core}(i,j)$ from the depth map τ_{core} of the plastic part.

The geometric layout of the straight-drilled channels from the nodes $\omega_{cavity}(i,j) \in \mathbb{R}^3$ and $\omega_{core}(i,j) \in \mathbb{R}^3$ of the $\mathcal{D}$' mesh is performed uniformly according to the technical and geometric parameters obtained in the optimization process of the physical model. To do this, the available domain from the nodes $\omega_{cavity}(i,j) \in \mathbb{R}^3$ and $\omega_{core}(i,j) \in \mathbb{R}^3$ and the required distance between each cooling channel L_b are evaluated as described in Appendix 7.1. The number and the uniform geometric layout of the perforated straight channels are also determined. The remaining parameters $D_{baffles}$ and L_p follow the physical model are described in Appendix 7.1. The functionality of perforated straight channels is therefore guaranteed since the application region $\omega_{cavity}(i,j) \in \mathbb{R}^3$ and $\omega_{core}(i,j) \in \mathbb{R}^3$ have depths $\tau_{cavity}(i,j) \in \mathbb{R}^3$ and $\tau_{core}(i,j) \in \mathbb{R}^3$, lower than the established limit values $L_{S_{cavity}}$ y $L_{S_{core}}$.

3.5. Boundary conditions

In the cavity and core plates of an injection mold several mechanical systems optimize the manufacturing process of the plastic part. The most important systems are the cooling and the ejection system of the plastic part. Therefore, for a properly geometrical design of the injection mold both systems (cooling and ejection) must be compatible and not create interferences between them. In this section, the defined a set of boundary conditions are established so that the design of the cooling system is compatible with the design of the ejection system.

3.5.1. *Interference between the cooling system and the ejection system*

The algorithm evaluates the interference between the cooling system and the ejection system of the plastic part for the core plate of the mold. To obtain the location of each ejector $\Phi_{ejector}(i,j)$ and its diameter $\emptyset_{ejector}$ the algorithm takes as input data the result of applying the procedure developed by the authors [32] to the $\mathcal{D}'$ mesh (see Fig 11) Eq.(21). Using this information, the algorithm detects and eliminates the nodes $\beta_{core}\ (i,j) \in \mathbb{R}^3$ that lie within the domain $\Delta_{ejec} \in \mathbb{R}^3$ defined as Eq.(22).

$$\forall\ \Phi_{ejector}(i,j)\ \exists\ \Delta_{ejec} \in \mathbb{R}^2 \mid A(\Delta_{ejec}) = (\emptyset_{ejector} + 2 \cdot L_p) \cdot w \quad (21)$$

$$\forall\ \beta_{core}\ (i,j) \in \mathbb{R}^3 \mid \beta_{core}\ (i,j) \in\ \Delta_{ejec} \rightarrow \beta_{core}\ (i,j) = \emptyset \quad (22)$$

Where $A(\Delta_{ejec})$ is the safety area around the ejectors, L_p is the safety distance on both sides of $\emptyset_{ejector}$ and w is the length of the Bounding Box of the part along the Y axis. The flat geometric region $\Delta_{ejec} \in \mathbb{R}^2$ is defined by the sum of the largest of the ejector diameters and the structural safety distance L_p (see Fig 11). In this way the design of the cooling system is linked to the ejection system, avoiding any type of interference between both that would compromise the structural safety of the mold.

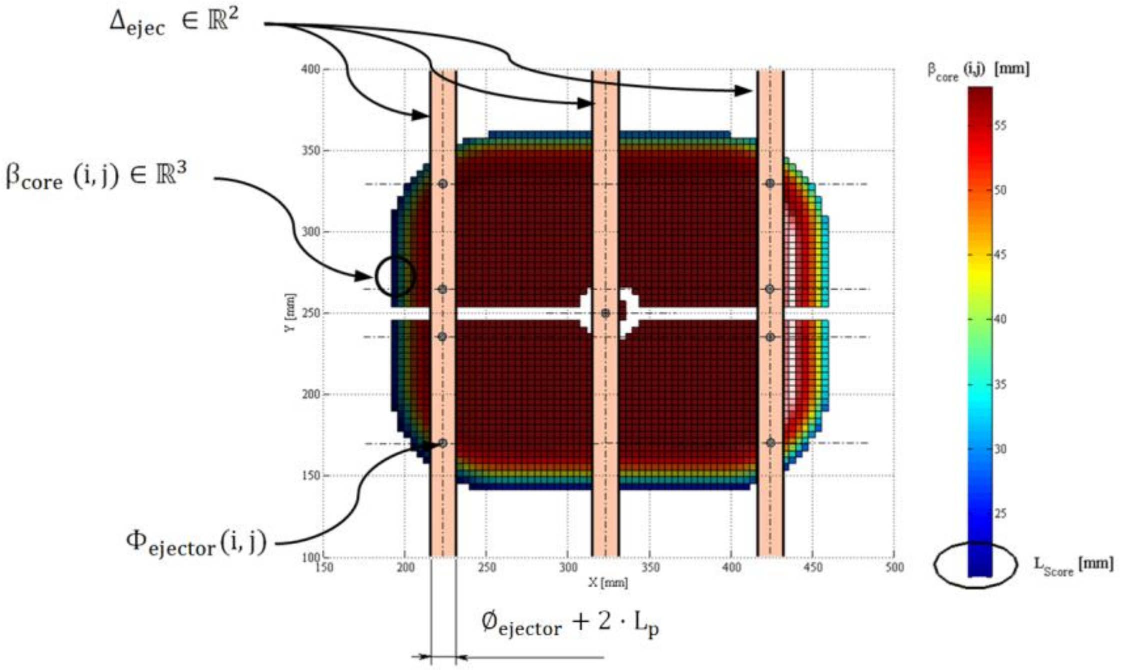

Fig. 11.- Resolution of the interference between the ejection system, $\Phi_{ejector}$, and the cooling system in core plate, β_{core}.

3.6. Baffles location via the genetic algorithm

After applying the boundary conditions on the set of nodes $\beta_{cavity} \in \mathbb{R}^3$ y $\beta_{core} \in \mathbb{R}^3$, this section establishes the location and final coordinates of the baffles of the cooling system. For this purpose the algorithm employs a genetic optimization algorithm that guarantees a balanced and uniform cooling system.

3.6.1. Initial Population

First, the population or the set of nodes from which the optimal solution will be obtained are determined. The set of nodes $\beta_{cavity} \in \mathbb{R}^3$ and $\beta_{core} \in \mathbb{R}^3$ is considered as the initial population. However, the algorithm performs a prior segmentation of the node population with the objective of reducing and optimizing both the execution time and the computational cost of the geometric optimization problem, guaranteeing the optimal solution of the problem. For this, the algorithm defines a sequence of 3D isocontours along the surface formed by $\beta_{cavity} \in \mathbb{R}^3$ and $\beta_{core} \in \mathbb{R}^3$, separated at equidistance D_p (see Fig 12a and 12b). The value of the parameter D_p is equal to the separation distance between baffles L_b plus their diameter $D_{baffles}$. The parameters L_b and $D_{baffles}$ related to the dimensioning of the cooling system have been defined in the paper in Appendix 7.1. The nodes that make up the initial population of study and that belong to the 3D isocontours are defined as $B_{cavity}(i,j) \in \mathbb{R}^3$ and $B_{core}(i,j) \in \mathbb{R}^3$, respectively. In Fig. 14a and 14b the 3D isocontours that make up the study population $B_{core} \in \mathbb{R}^3$ are indicated.

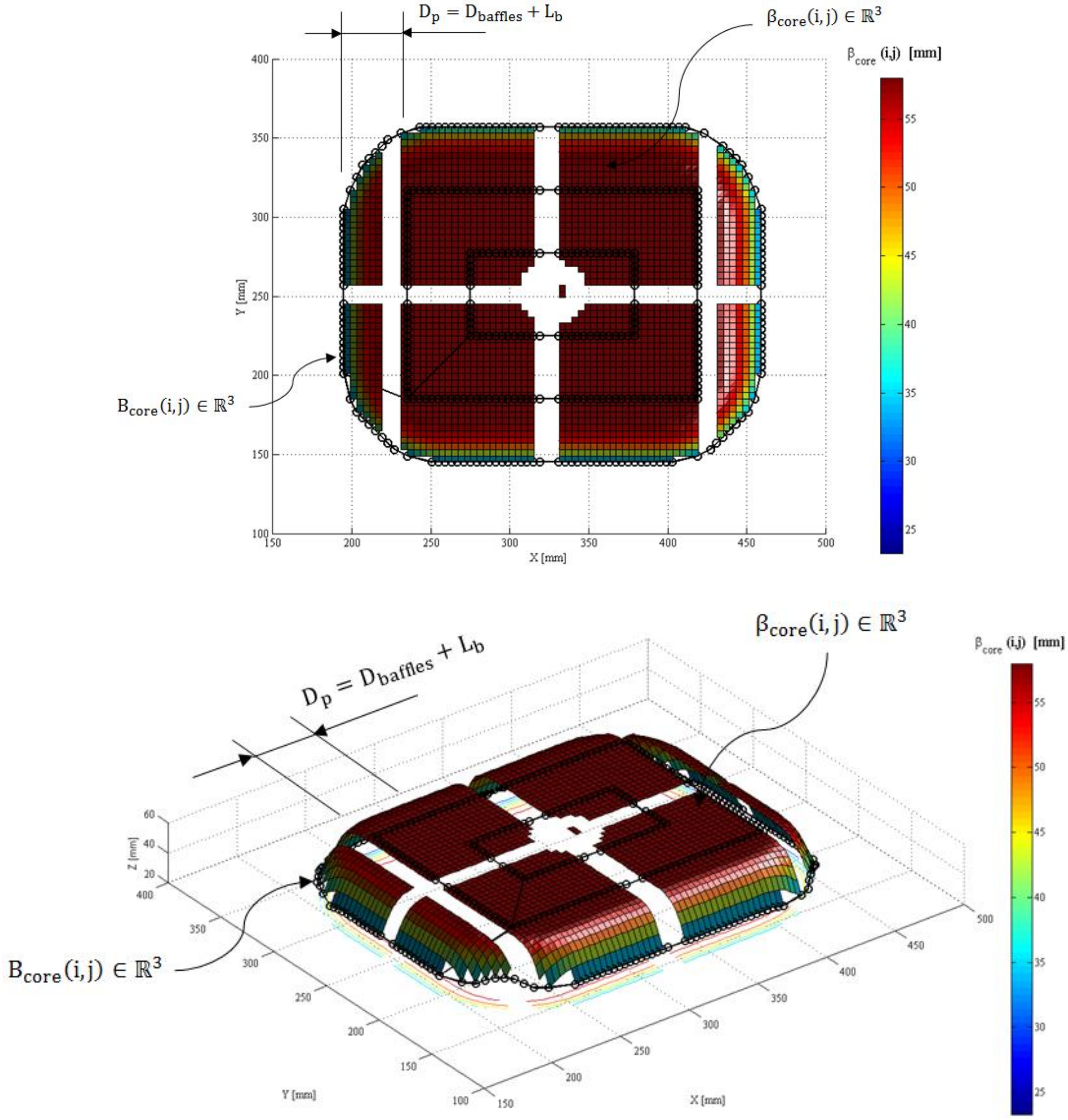

Figs. 12a and 12b.- Representation by isocontours 3D of β_{core} nodes of the initial population, B_{core}.

3.6.2. *Number of variables*

The next step of the geometric problem posed is to determine the number of variables. The number of variables is directly proportional to the number of baffles that form the cooling system of the mold. In order to obtain a uniform temperature map on the surface of the cavities that will mold part $\mathcal{D}$, the number of baffles of the cooling system must be maximum. Thus, on each node belonging to $B_{cavity}\,(i,j) \in \mathbb{R}^3$ and $B_{core}(i,j) \in \mathbb{R}^3$, the center of a circle $r_p(i,j) \in \mathbb{R}^2$, with radius equal to $D_p/2$, where D_p is the distance between each 3D isocontour, $B_{cavity}\,(i,j) \in \mathbb{R}^3$ and $B_{core}(i,j) \in \mathbb{R}^3$. Next, the number of nodes of the 3D isocontours, $B_{cavity} \in \mathbb{R}^3$ or $B_{core} \in \mathbb{R}^3$ contained within each circular circular contour $r_p(i,j) \in \mathbb{R}^2$, except for the node of analysis $B_{cavity}(i,j) \in \mathbb{R}^3$ or $B_{core}(i,j) \in \mathbb{R}^3$ is determined. All nodes $B_{core}(i,j) \in \mathbb{R}^3$ y $B_{cavity}(i,j) \in \mathbb{R}^3$ that meet the geometric condition of being located within the circular contour $r_p(i,j) \in \mathbb{R}^2$ will be removed from the count. On the contrary, $B_{cavity}(i,j) \in \mathbb{R}^3$ or $B_{core}(i,j) \in \mathbb{R}^3$ nodes that do not meet the location condition within the locus $r_p(i,j) \in \mathbb{R}^2$ will continue to form part of the analysis.

In Fig 13, an example of locating a circle $r_p(i,j)$ from a node $B_{core}\,(i,j)$ of the geometric region β_{core} is indicated.

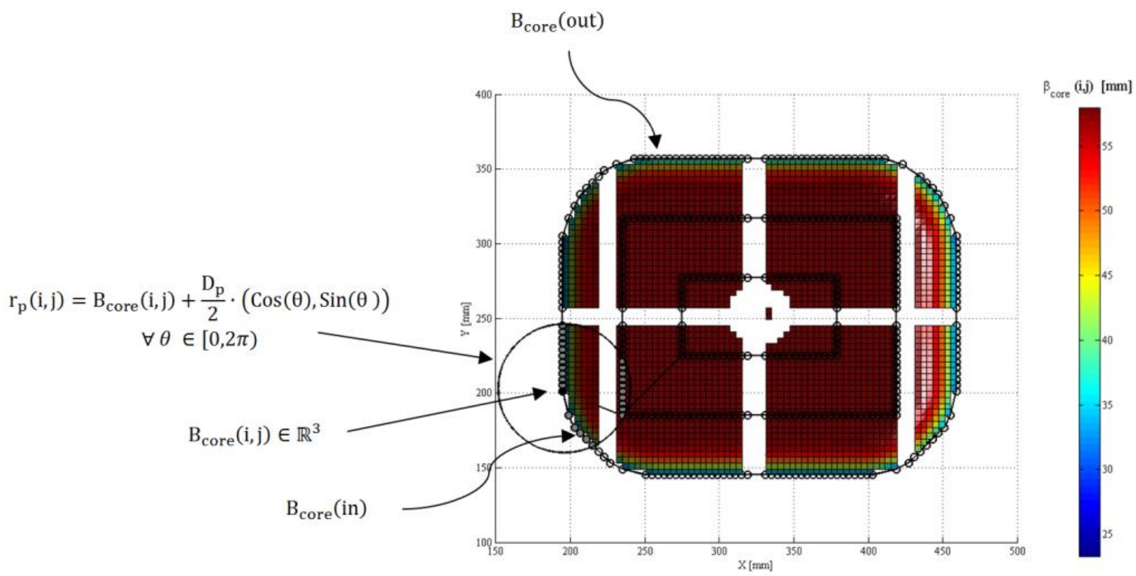

Fig. 13.- Representation of a circle $r_p(i,j)$ from a node $B_{core}\ (i,j)$ of the geometric region β_{core} .

After applying this condition to each node $B_{cavity} \in \mathbb{R}^3$ and $B_{core} \in \mathbb{R}^3$, the total number of baffles is obtained for the layout for both the cavity plate and the core plate cooling system. The resulting total number of baffles is equal to the number of nodes $B_{cavity}(i,j) \in \mathbb{R}^3$ and $B_{core}(i,j) \in \mathbb{R}^3$ that have met the imposed geometric condition of being located within the contour of one of the circumferences $r_p(i,j) \in \mathbb{R}^2$Eq.(23).

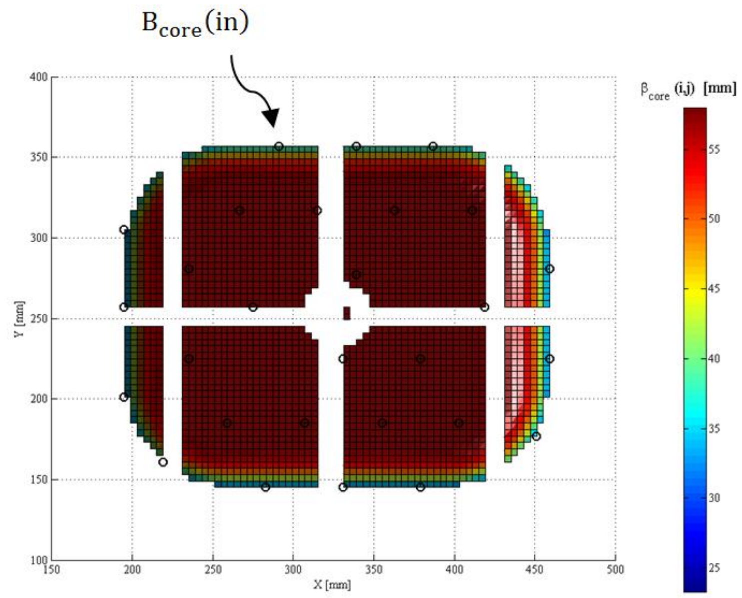

Fig. 14.- Nodes $B_{core}\ (i,j)$ that do not meet the condition of being contained in the circular regions $r_p(i,j)$.

$$n_{blaffes_{cavity}} = size(B_{cavity(in)})$$

$$n_{blaffes_{core}} = size(B_{core(in)}) \tag{23}$$

Fig. 14 shows the set of nodes $B_{core}(i,j) \in \mathbb{R}^3$ that have not met the proposed condition. As can be seen, the location of these points is not balanced or uniform, but the total number of these points allows the number of variables of the optimization problem to be determined. Since the variables of the geometric optimization problem represent the coordinates of the geometric center of the different baffles in the coordinate axes X, Y, the final number of variables to be optimized will be equal to twice the maximum number of baffles with which the cooling system is designed for the cavity and core plate, respectively. Thus, the problem variables correspond to the X and Y (xcore, ycore), (x_{cavity}, y_{cavity}) coordinates of the center of each of the baffles.

Nomenclature	Units	Description	Notation on the optimization problem
x_{cavity}	mm	X coordinates vector of cavity plate baffles	$\mathrm{x(1)} = \left\{\mathrm{x_{cavity}(1)} \quad \dots \quad \mathrm{x_{cavity}}\left(\mathrm{n_{blaffes_{cavity}}}\right)\right\}$
y_{cavity}	mm	Y coordinates vector of cavity plate baffles	$\mathrm{x(2)} = \left\{\mathrm{y_{cavity}(1)} \quad \dots \quad \mathrm{y_{cavity}}\left(\mathrm{n_{blaffes_{cavity}}}\right)\right\}$
x_{core}	mm	X coordinates vector of core plate baffles	$\mathrm{x(3)} = \{\mathrm{x_{core}(1)} \quad \dots \quad \mathrm{x_{core}}(\mathrm{n_{blaffes_{core}}})\}$
y_{core}	mm	Y coordinates vector of core plate baffles	$\mathrm{x(4)} = \{\mathrm{y_{core}(1)} \quad \dots \quad \mathrm{y_{core}}(\mathrm{n_{blaffes_{core}}})\}$

Constrains
$\min\left(B_{cavity}\right)_{\mathrm{x}} \leq \mathrm{x(1)} \leq \max\left(B_{cavity}\right)_{\mathrm{x}}$
$\min\left(B_{cavity}\right)_{\mathrm{y}} \leq \mathrm{x(2)} \leq \max\left(B_{cavity}\right)_{\mathrm{y}}$
$\min(B_{core})_{\mathrm{x}} \leq \mathrm{x(3)} \leq \max(B_{core})_{\mathrm{x}}$
$\min(B_{core})_{\mathrm{y}} \leq \mathrm{x(4)} \leq \max(B_{core})_{\mathrm{y}}$

Table 3.- Variables of the geometric optimization problem.

3.6.3. *Options structure and Fitness functions*

To complete the definition of the optimization problem posed in this section, the rest of the configuration parameters are detailed in table 4.

Genetic Algorithm Options Structure	Defined Set-up
Population	Double Vector. The set of nodes that are part of the initial population are $B_{cavity,core} \in \mathbb{R}^3$, respectively. See Fig 13 a, b.
Scaling Function	Fitness Rank
Selection	Uniform Stochastic
Reproduction	Two Points
Mutation	20%
Crossove factor	80%
Migration	Direction: Both ; Migration Interval: 1 ; Migration factor: 0.8

Table 4.-. Definition of the geometric optimization problem.

The constraints have been set according to the maximum and minimum values of the coordinates of the set of nodes $B_{cavity} \in \mathbb{R}^3$ or $B_{core} \in \mathbb{R}^3$ in the coordinate axes X, Y in order to prevent the solution from converging outside the domain of analysis. To complete the multiobjective optimization problem, the fitness functions to optimize must be entered. First, the optimization algorithm developed in the paper employs a fitness function to ensure that the geometric centers of the baffles are separated from each other at a distance greater than the minimum estimated separation D_p Eq.(27).

The sets of solution nodes are called $P_{baffle_{cavity}} \in \mathbb{R}^3$ and $P_{baffle_{core}} \in \mathbb{R}^3$ Eq.(25). Each solution node $P_{baffle_{cavity}}(i,j) \in \mathbb{R}^3$ and $P_{baffle_{core}}(i,j) \in \mathbb{R}^3$ (see Fig 15) has associated a distance $d_{baffles_{cavity}}(i,j)$ and $d_{baffles_{core}}(i,j)$ representing the separation between that node and the nearest solution node Eq.(24). Thus, if all the distances are equal or greater than $\mathrm{D_p}$ the fitness function takes a minimum value equal to 0 and otherwise takes maximum values equal to infinity Eq.(26).

$$\mathrm{P_{baffle_{cavity}}(i,j)} = \left\{\mathrm{x_{cavity}(i,j)_x} \quad \mathrm{y_{cavity}(i,j)_y} \quad \mathrm{z_{cavity}(i,j)_z} - \mathrm{L_p}\right\}$$

$$\mathrm{P_{baffle_{core}}(i,j)} = \{\mathrm{x_{core}(i,j)_x} \quad \mathrm{y_{core}(i,j)_y} \quad \mathrm{z_{core}(i,j)_z} - \mathrm{L_p}\} \tag{24}$$

The Z coordinate of the solution points $P_{baffle_{cavity}}(i,j) \in \mathbb{R}^3$ and $P_{baffle_{core}}(i,j) \in \mathbb{R}^3$ is obtained by projecting solution $P_{baffle_{cavity}}(i,j) \in \mathbb{R}^3$ and $P_{baffle_{core}}(i,j) \in \mathbb{R}^3$ on the surface formed by the set of nodes $\beta_{cavity} \in \mathbb{R}^3$ and $\beta_{core} \in \mathbb{R}^3$. According to the structural safety requirements established in this paper, the magnitude of the coordinates in the Z axis of the solution points are subtracted by the structural safety distance L_p.

$$\forall\ P_{baffle_{cavity}}(i,j) \in \mathbb{R}^3\ \exists\ d_{baffles_{cavity}}(i,j)$$

$$\forall\ P_{baffle_{core}}(i,j) \in \mathbb{R}^3\ \exists\ d_{baffles_{core}}(i,j) \quad (25)$$

$$\text{If all}\left(d_{baffles_{cavity}}\right) \geq D_p \rightarrow f_{1_{cavity}} = 0\ ;\ \text{else} \rightarrow f_{1_{cavity}} = \text{Inf}$$

$$\text{If all}\left(d_{baffles_{core}}\right) \geq D_p \rightarrow f_{1_{core}} = 0\ ;\ \text{else} \rightarrow f_{1_{core}} = \text{Inf} \quad (26)$$

$$\text{Fitness Function}_1\text{: Min}\{f_{1_{cavity}} \quad f_{1_{core}}\} \quad (27)$$

Secondly, in order to favor heat exchange in regions with greater concavity, the sum of the Z coordinates of the solution nodes $P_{baffle_{cavity}} \in \mathbb{R}^3$ and $P_{baffle_{core}} \in \mathbb{R}^3$ must be maximum Eq.(28).

$$\text{Fitness Function}_2\text{: Max}\{z_{cavity}(i,j)_z \quad z_{core}(i,j)_z\} \quad (28)$$

Thirdly, in order to obtain a balanced cooling system design the distance between the projection in the XY plane of the mass center of the solution nodes (baffles geometric center) and the projection in the XY plane of the mass center of the plastic part should be minimal.

$$CM_{baffle_{cavity}} = \left[\frac{\sum x_{cavity}(i,j)}{\text{size}(x_{cavity})} \quad \frac{\sum y_{cavity}(i,j)}{\text{size}(y_{cavity})}\right]$$

$$CM_{baffle_{core}} = \left[\frac{\sum x_{core}(i,j)}{\text{size}(x_{core})} \quad \frac{\sum y_{core}(i,j)}{\text{size}(y_{core})}\right]$$

(29)

$$\text{Fitness Function}_3\text{: Min}\{|CM_{baffle_{cavity}} \quad CM_{xy}| \quad |CM_{baffle_{core}} \quad CM_{xy}|\} \quad (30)$$

Finally, in order to obtain a uniform cooling system design the variance Eqs.(33)-(36) of the distances between baffles in the coordinate axes X, Y must be minimal Eq.(32). Each solution point $P_{baffle_{cavity}}(i,j) \in \mathbb{R}^3$ and $P_{baffle_{core}}(i,j) \in \mathbb{R}^3$ has associated a vector of distance $d_{baffles_{cavity}}(i,j)_{x,y}$ and $d_{baffles_{core}}(i,j)_{x,y}$ representing the separation distance between that node and the solution node closest to it in the coordinate axes X, Y Eq.(31). In the case where a pair of nodes are aligned with each other on a coordinate axis, the distance between them is assigned as 0. Fig 15 shows the definition of the distance vectors $d_{baffles_{cavity}}(i,j)_{x,y}$ and $d_{baffles_{core}}(i,j)_{x,y}$ on the final solution of the geometric optimization problem.

$$\forall\ P_{baffle_{cavity}}(i,j) \in \mathbb{R}^3\ \exists\ d_{baffles_{cavity}}(i,j)_{x,y}$$

$$\forall\ P_{baffle_{core}}(i,j) \in \mathbb{R}^3\ \exists\ d_{baffles_{core}}(i,j)_{x,y} \quad (31)$$

$$\text{Fitness Function}_4\text{: Min}\left\{\text{Var}\left(d_{baffles_{cavity_{x,y}}}\right) \quad \text{Var}\left(d_{baffles_{core_{x,y}}}\right)\right\} \quad (32)$$

$$\text{Var}\left(d_{baffles_{cavity_{x,y}}}\right) = \frac{1}{\text{size}(d_{baffles_{cavity_{x,y}}})} \cdot \sum_{i=1}^{\text{size}(d_{baffles_{cavity_{x,y}}})} \left|d_{baffles_{cavity_{x,y}}}(i) - \mu_{baffles_{cavity_{x,y}}}\right|^2$$

(33)

Where

$$\mu_{baffles_{cavity_{x,y}}} = \frac{1}{\text{size}(d_{baffles_{cavity_{x,y}}})} \cdot \sum_{i=1}^{\text{size}(d_{baffles_{cavity_{x,y}}})} d_{baffles_{cavity_{x,y}}}(i)$$

(34)

Similarly for the solution corresponding to the core plate Eqs. (35)-(36).

$$\text{Var}\left(d_{baffles_{core_{x,y}}}\right) = \frac{1}{\text{size}(d_{baffles_{core_{x,y}}})} \cdot \sum_{i=1}^{\text{size}(d_{baffles_{core_{x,y}}})} \left|d_{baffles_{core_{x,y}}}(i) - \mu_{baffles_{core_{x,y}}}\right|^2$$

(35)

Where.

$$\mu_{baffles_{core_{x,y}}} = \frac{1}{size(d_{baffles_{core_{x,y}}})} \cdot \sum_{i=1}^{size(d_{baffles_{core_{x,y}}})} d_{baffles_{core_{x,y}}}(i)$$

(36)

In addition, in order for the solution to encompass the maximum domain $\beta_{cavity} \in \mathbb{R}^3$ and $\beta_{core} \in \mathbb{R}^3$, the difference between the sum of the distance vectors $d_{baffles_{cavity}}(i,j)_{x,y}$ and $d_{baffles_{core}}(i,j)_{x,y}$ and the lengths of the Bounding Box of the plastic part l and w must be minimal (The definition of the Bounding Box of the plastic part has been detailed in section 3.2) Eq.(37).

$$\text{Fitness Function}_5\text{: Min}\begin{Bmatrix} \sum d_{baffles_{cavity_x}}(i,j) - l & \sum d_{baffles_{cavity_y}}(i,j) - w \\ \sum d_{baffles_{core_x}}(i,j) - l & \sum d_{baffles_{core_y}}(i,j) - w \end{Bmatrix}$$

(37)

After the application of the optimization algorithm in Fig 16, the result of the geometric centers of the baffles $P_{baffle_{core}}(i,j) \in \mathbb{R}^3$ is presented. As shown in Fig. 16, the cavity plate does not require the use of baffles for the design of the cooling system. The entire domain of $\beta_{cavity} \in \mathbb{R}^3$ meets the boundary conditions detailed in section 3.4.2 and therefore $\beta_{cavity} \in \mathbb{R}^3$ results in an empty set with respect to the number of baffles. The modeling of the cooling system for the cavity plate is carried out through evenly distributed horizontal channels, according to the technical and geometric parameters obtained in section 3.3.

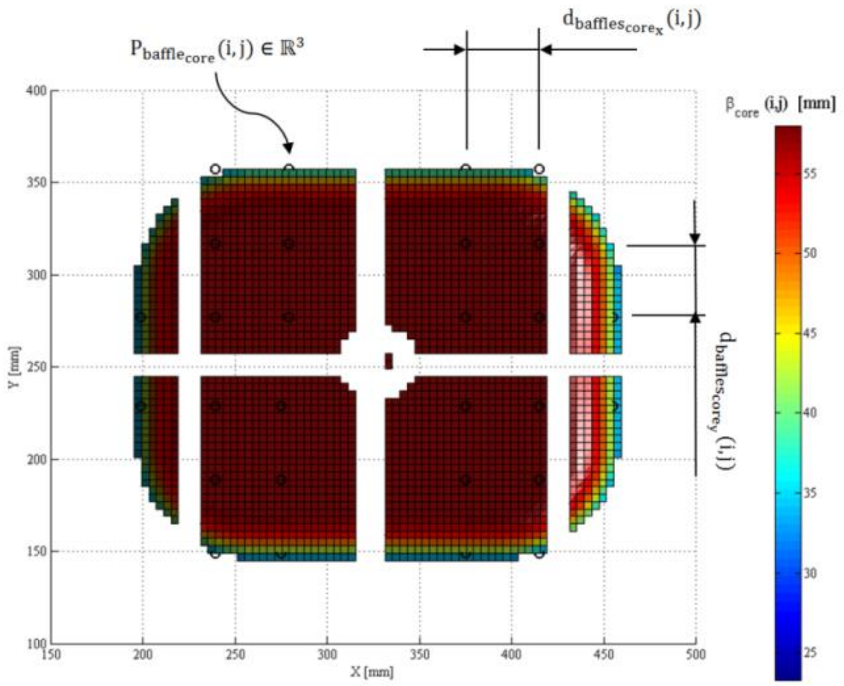

Fig. 15.- Location of solution nodes $P_{baffle_{core}}(i,j)$ and representation of separating distances $d_{baffles_{core}}(i,j)_{x,y}$.

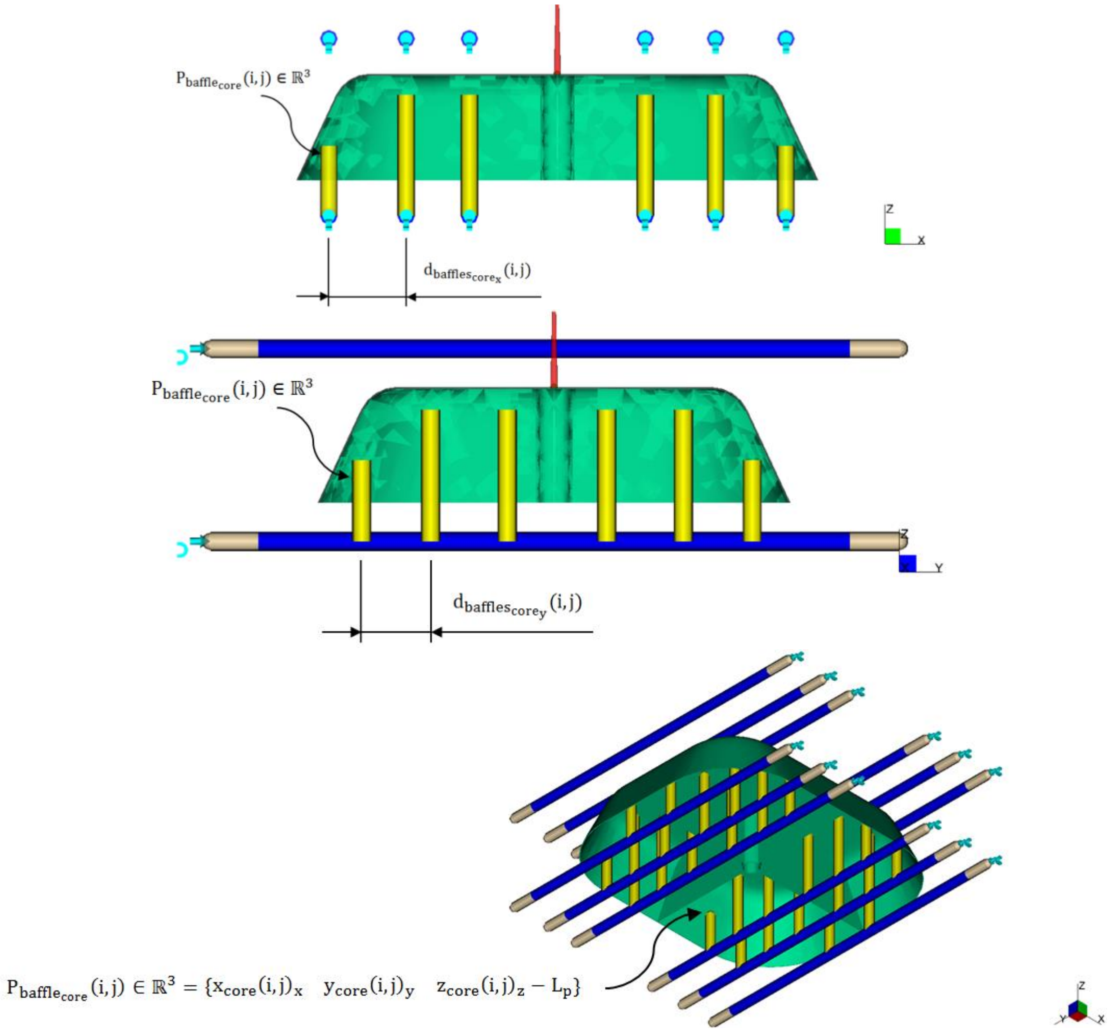

Fig. 16.- Solution for the design of the cooling system for part $\mathcal{D}$.

Fig. 16 shows the design of the resulting cooling system after applying the algorithm to the plastic part $\mathcal{D}$. The coordinates of the geometric centers of the baffles, and the calculated technical and geometric parameters $\overline{T_m}$ [ºC], T_c[ºC], L_b [mm] and $D_{baffles}$ [ºC] are exported to a calculation software with the objective of performing a simulation in order to validate and verify the efficiency and performance of the proposed model.

4. Implementation and results

In order to demonstrate the benefit of the algorithm proposed in this paper it has been applied to four industrial parts with complex shapes, manufactured by means of the plastic injection process. The accuracy of the nodal mesh (ε) for each geometry is set according to the dimension of the smallest detail of the part. The algorithms have been developed in the software Matlab R2013a [35] with a Toshiba notebook with a Pentium (R) Dual-Core CPU T4200@2.20 GHz processor and a RAM memory of 3.00 GB.

The proposed method generates an automatic cooling system design without the need for post-processing operations. In addition, the arrangement of the elements of the cooling system and its technical parameters are automatically defined. The simulations carried out to validate the proposed algorithm have been performed using the injection molding simulation software MoldFlow Advisor [36]. The proposed methodology generates a resulting array that includes: the coordinates X, Y, Z of the points defining the baffles, the diameter of the cooling system elements, the mold surface temperature and the coolant temperature. This information is imported into Moldflow to generate and size the main cooling channels and baffles of the mold cooling system. Acrylonitrile butadiene styrene (ABS) is used as the thermoplastic part material and structural steel (P20) is employed as the material for the plates and components of the injection mold. The materials used for the validation of the proposed algorithm are given in Table 5a, b and Table 6. The coolant used is water and the value of the nominal flow used is that which maintains the additional Reynolds number equal to $1.5 \cdot 10^4$ (turbulent flow), and the inlet temperature of the coolant is obtained as a result of the proposed algorithm.

Material: ABS	Nomenclature	Value	Units
Melt Density	ρ_c	0.979	kg/mm^3
Melt Specific Heat	c_p	2012	J/kg·ºC
Latent heat of fusion of the polymer	i_m	130000	J/kg
Melt Temperature	T_{melt}	270	ºC
Ejection Temperature	T_{eject}	135	ºC

Table 5a.-Material properties of the plastic part.

Material: Structural Steel P-20	Nomenclature	Value	Units
Thermal conductivity	δ_s	45	W/m·ºC
Heat transfer coefficient between mold and coolant	h	4500	W/m^2·ºC
Thermal diffusivity	α_s	$8.73\cdot10^{-8}$	m^2/s

Table 5b.-Material properties of the injection mold.

Both the injection temperature and the ejection temperature are assumed to be uniform throughout the analytical study presented in this paper. The value of each of these parameters is determined by the manufacturer as standard quantities for correct injection and subsequent ejection of the thermoplastic material.

	Units	Case study A	Case study B	Case study C	Case study D
Bounding Box	mm^3	[300-250-60.5]	[350-600-50]	[670-240-114]	[300-250-60]
Thickness	mm	1	3	2	3
Volume	mm^3	122721.9	984119.1	6498773.9	374188.6
Cavity plate area	mm^2	99013.8	375520.8	364571.8	81802.8
Core plate area	mm^2	156835.0	247481.7	327056.7	166755.2

Table 6.-Geometry properties of plastic parts.

4.1. Case studies

The results of applying the proposed algorithm for the four plastic parts (Case A, B, C, D) Figs 17, 23, 29 and 35 are shown in Figs 18, 24, 30 and 36. The geometric distribution and location of the baffles and the main cooling channels and the value of their diameters are calculated automatically. Furthermore, the temperature and pressure distribution of the coolant (Figs 19, 25, 31, 37), the temperature map for each plastic part (Figs 20, 26, 32, 38) and the cycle time map or time to reach ejection temperature (Figs. 22, 28, 34, 40) were added for the validation of each case study. The results of the algorithm for each plastic part are shown in Tables 7, 8, 9 and 10 that contain the diameter of the cooling channels and baffles $D_{baffles}$ [mm], the separation distance between baffles L_b[mm], the cooling quality of the system as a percentage, the temperature of the cooling fluid T_c [ºC], the average time needed to reach ejection temperature t_{cycle} [s] and the average mold cavity surface temperature $\overline{T_m}$ [ºC]. The values of these last two parameters are shown for both the analytical solution of the proposed algorithm and the solution obtained by means of the injection molding simulation software. In order to evaluate the quality of the final product and the cooling system, Figs. 21, 27, 33 and 39 show the quality obtained by each plastic part after the cooling phase. All this, together with the comparison of results obtained through the proposed algorithm and through the injection molding simulation software, allow us to determine that the results obtained by the methodology described in this paper are adapted to the design criteria of cooling systems of the plastic parts. The efficiency of the algorithm is demonstrated for parts with large concavities, slender details, internal turrets and housings.

The solutions obtained by this methodology are dimensioned under four objectives: minimizing the difference between the mold cavity surface temperature obtained by means of the optimization problem and the resulting magnitude according to the physical model, maximizing the distance between baffles, minimizing the diameter of the cooling channels and the cycle time. In addition, the geometric solution of the cooling system meets four design conditions: the distance between baffles is greater than the minimum safety distance between mold elements D_p [mm], the location of the baffles is guaranteed for deeper regions of the part (regions difficult to cool), and the resulting system is balanced and uniformly distributed along the geometry of the plastic part.

4.1.1. Case A

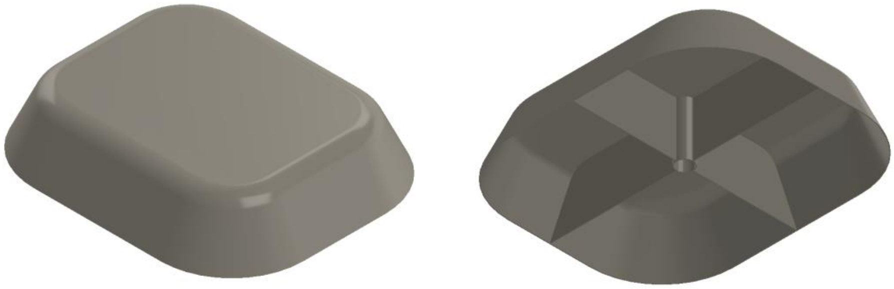

Fig. 17.- Plastic part, Case A.

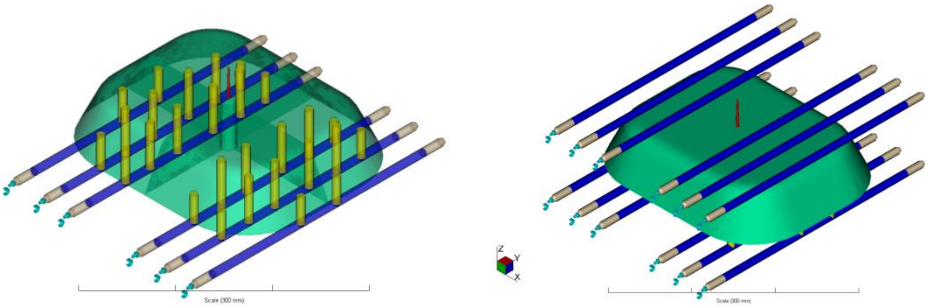

Fig. 18.- Geometric solution of the hybrid cooling system design, Case A.

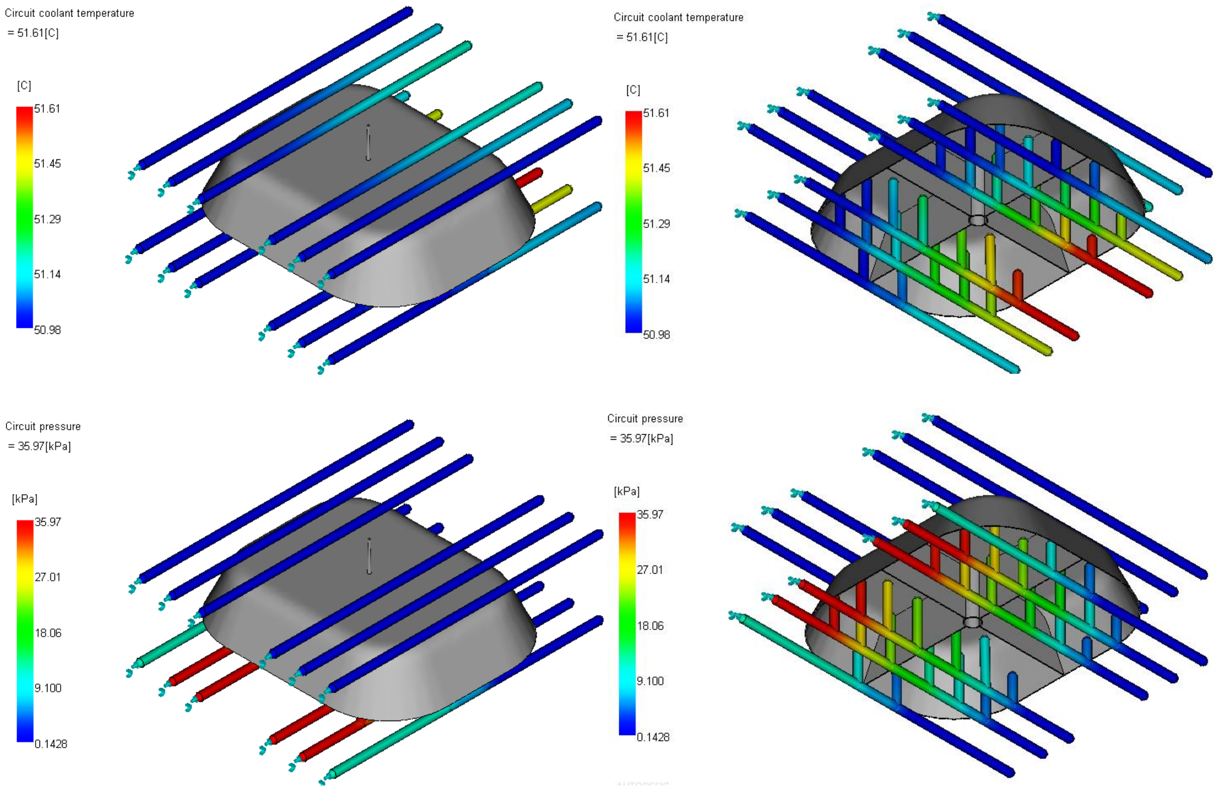

Fig. 19.- Distribution of the pressure field [kPa] and temperatures [°C] of the coolant along the cooling system, Case A.

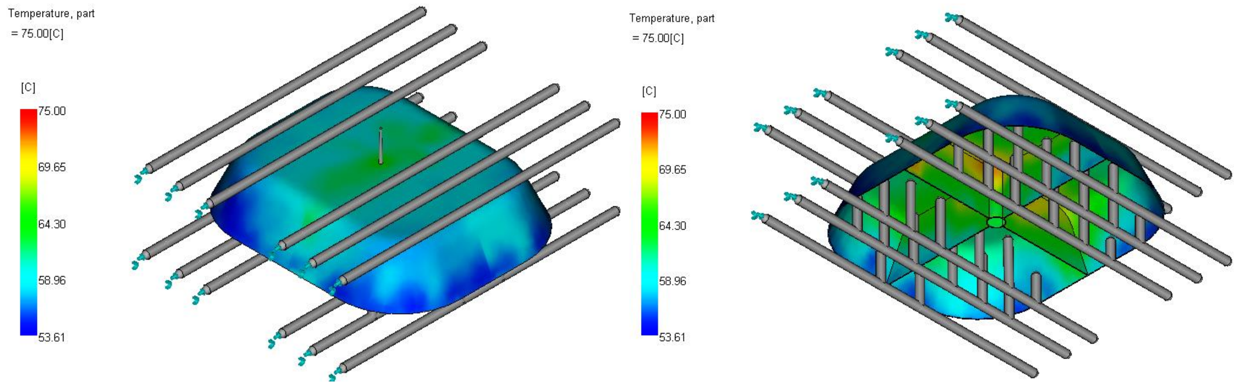

Fig. 20.- Distribution of the average temperature field at the surface of the plastic part during the cooling phase, Case A.

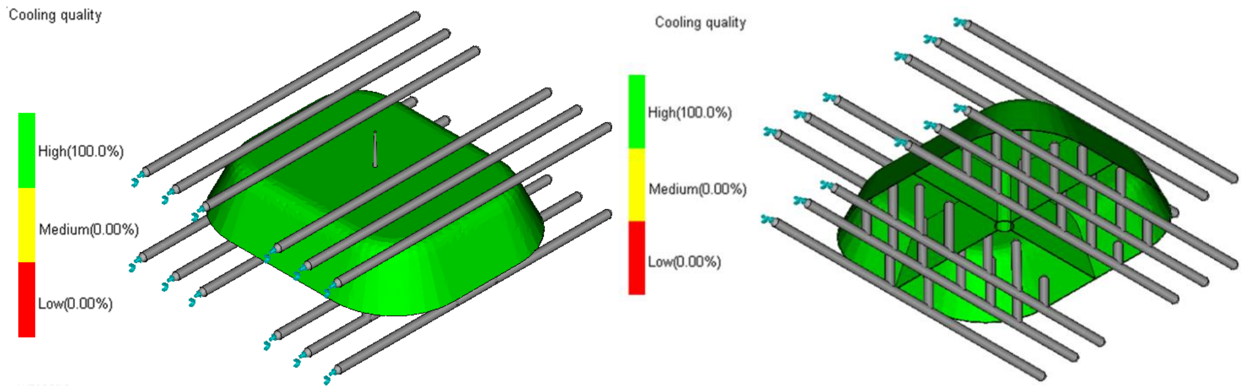

Fig. 21.- Final quality of cooling along the geometry of the plastic part, Case A.

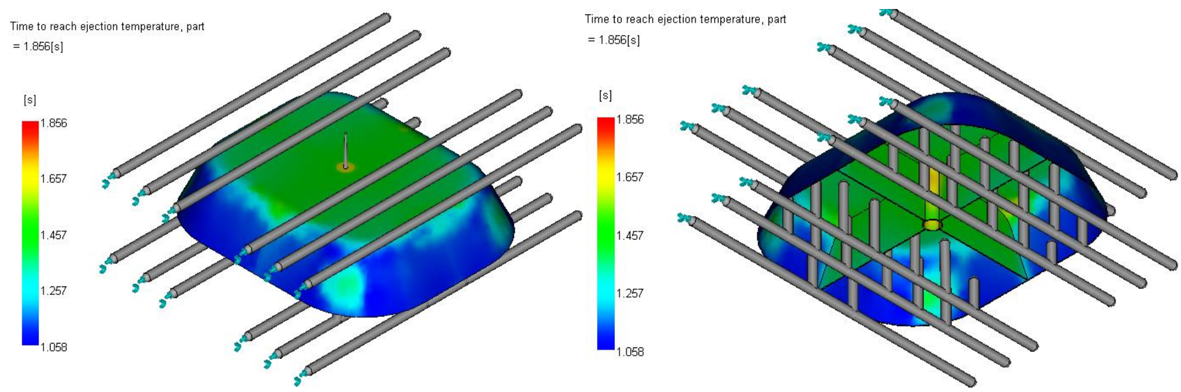

Fig. 22.- Distribution of the cycle time [s] or time until reaching the ejection temperature on the surface of the plastic part, Case A.

Nomenclature	Units	Description	Analytical algorithm	Injection molding simulation
$\overline{T_m}$	ºC	Average mold cavity surface temperature	61.5	60.3
T_c	ºC	Coolant temperature	51.3	51.0
t_{cycle}	s	Average time required to reach ejection temperature	1.2	1.4
Q	-	Cooling quality	-	100 %
L_b	mm	Distance between baffles	30	30
$D_{baffles}$	mm	Diameter of cooling channels	10	10

Table 7.-Results of the algorithm for Case A: Average mold cavity surface temperature ($\overline{T_m}$) [ºC], coolant temperature (T_c) [ºC], average time required to reach ejection temperature (t_{cycle}) [s], coolant quality, distance between baffles (L_b) [mm] and diameter of cooling channels ($D_{baffles}$) [mm].

4.1.2. Case B

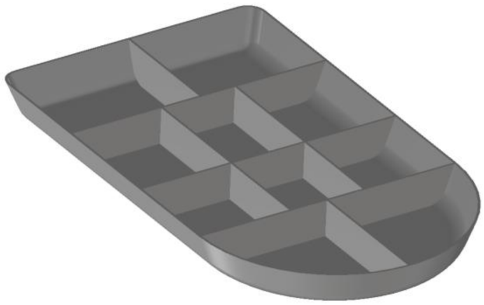

Fig. 23.- Plastic part, Case B.

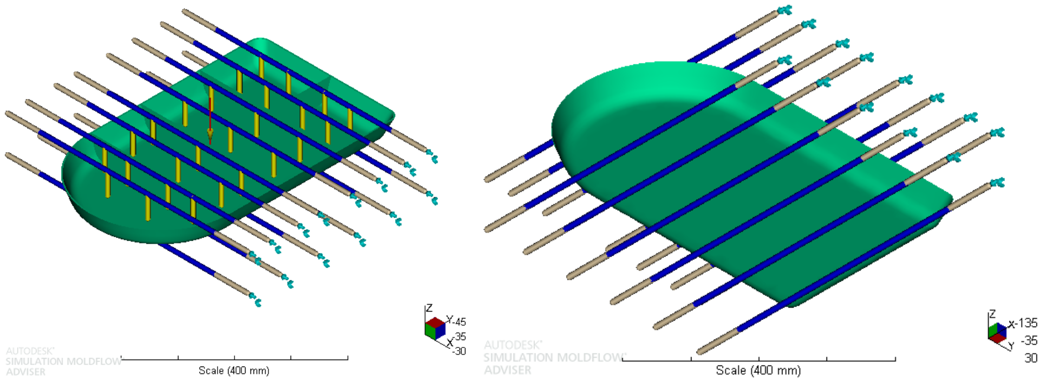

Fig. 24.- *Geometric solution of the hybrid refrigeration system design, Case B.*

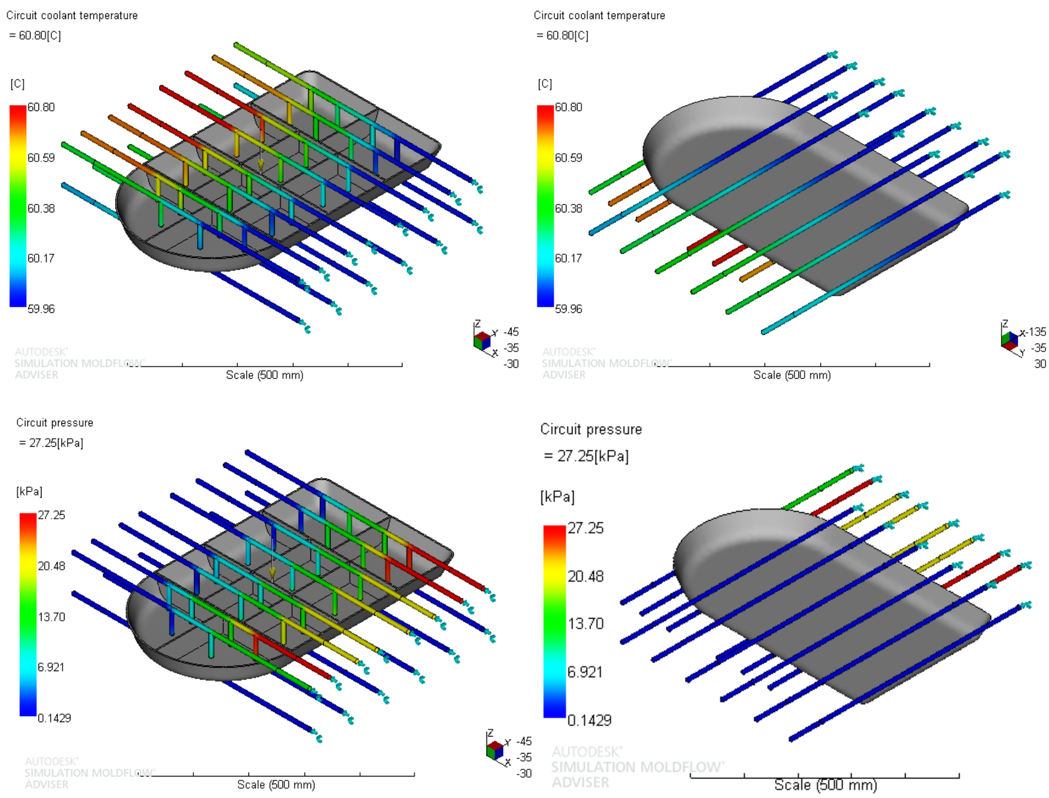

Fig. 25.- Distribution of the pressure field [kPa] and temperatures [° C] of the cooling fluid throughout the cooling system, Case B.

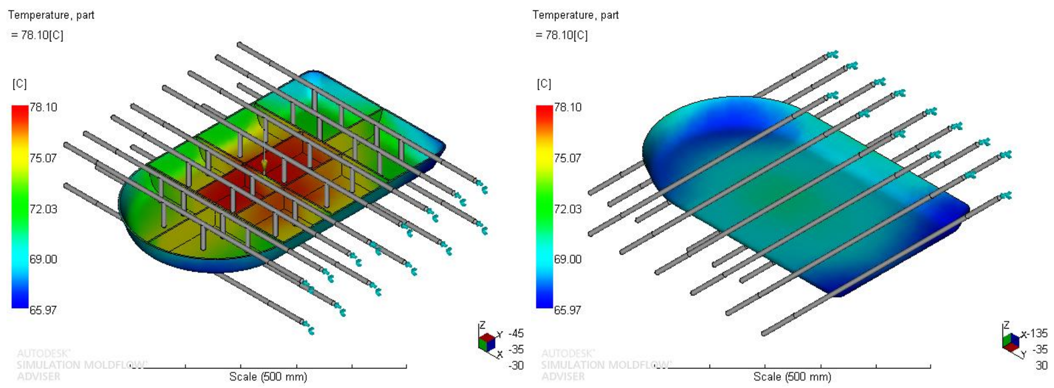

Fig. 26.- Distribution of the mean temperature field at the surface of the plastic part during the cooling phase, Case B.

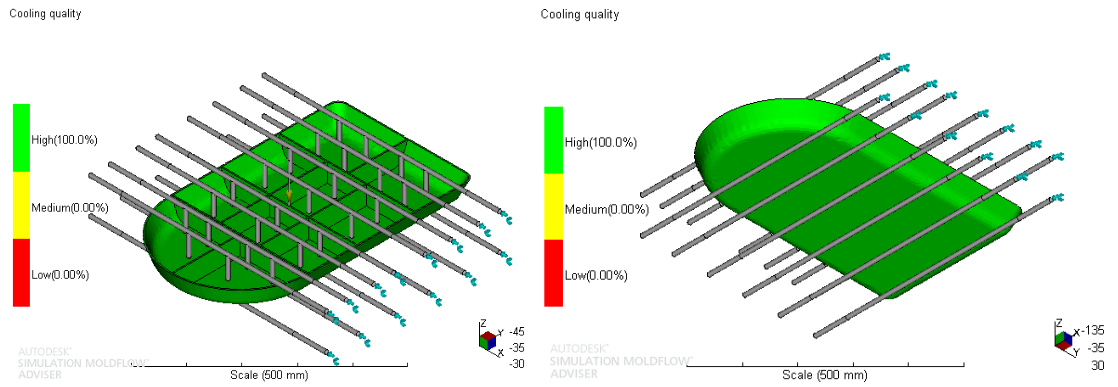

Fig. 27.- Final quality of cooling along the geometry of the plastic piece, Case B.

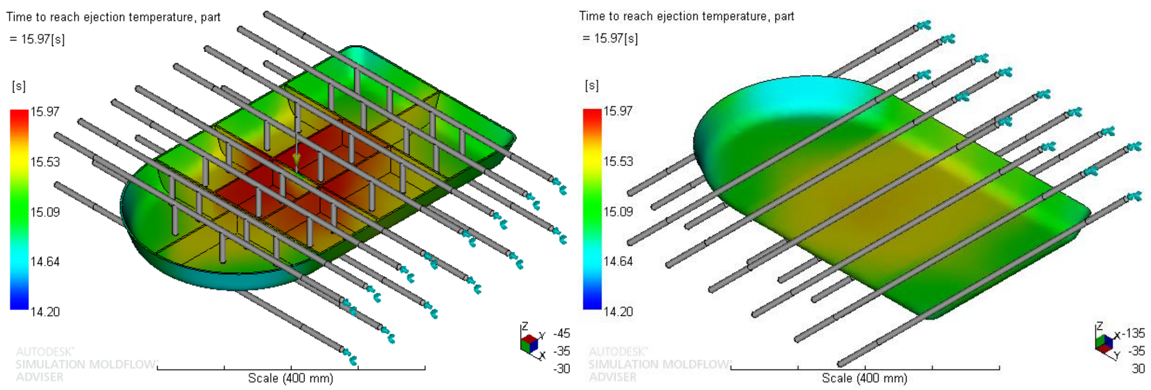

Fig. 28.- Cycle time distribution [s] or time until the ejection temperature is reached on the surface of the plastic part, Case B.

Nomenclature	Units	Description	Analytical algorithm	Injection molding simulation
$\overline{T_m}$	ºC	Average mold cavity surface temperature	74.4	78.7
T_c	ºC	Coolant temperature	60.7	60.0
t_{cycle}	s	Average time required to reach ejection temperature	14.8	15.1
Q	-	Cooling quality	-	100 %
L_b	mm	Distance between baffles	65	65
$D_{baffles}$	mm	Diameter of cooling channels	10	10

Table 8.- Results of the algorithm for Case B: Average mold cavity surface temperature ($\overline{T_m}$) [ºC], coolant temperature (T_c) [ºC], average time required to reach ejection temperature (t_{cycle}) [s], coolant quality, distance between baffles (L_b) [mm] and diameter of cooling channels ($D_{baffles}$) [mm].

4.1.3. Case C

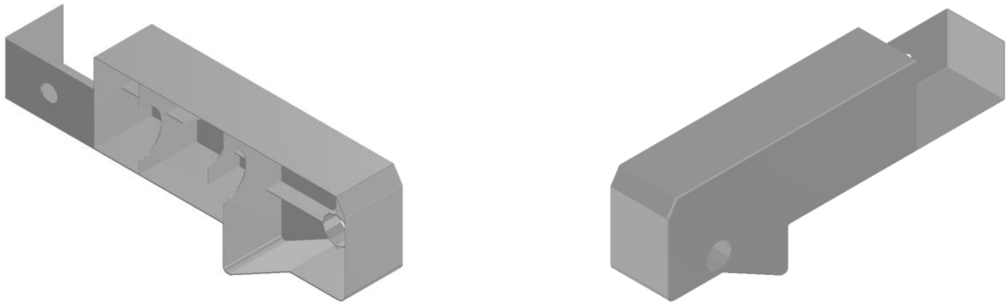

Fig. 29.- Plastic part, Case C.

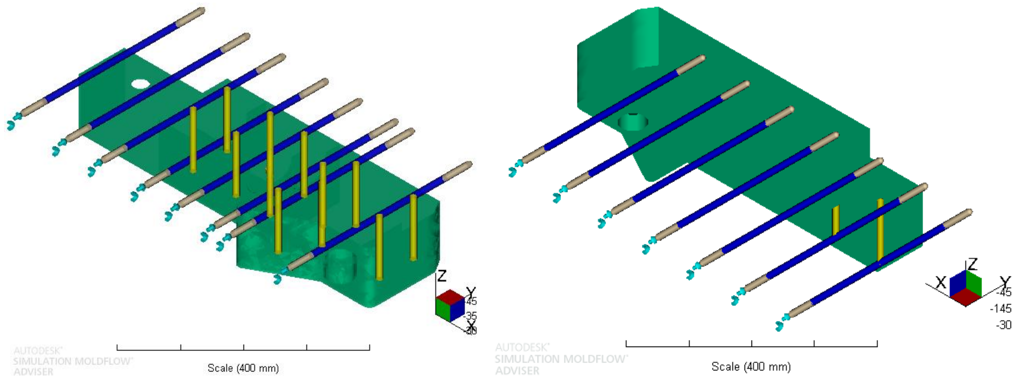

Fig. 30.- Geometric solution of the hybrid cooling system design, Case C.

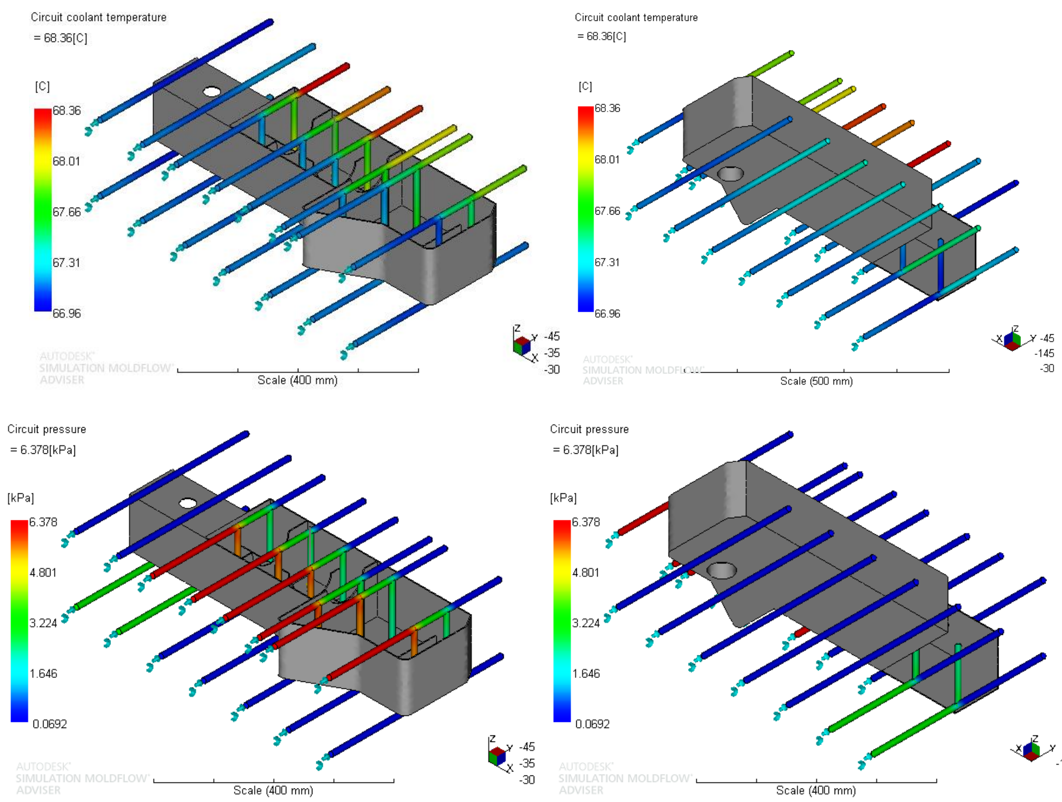

Fig. 31.- Distribution of the pressure field [kPa] and temperatures [° C] of the cooling fluid throughout the cooling system, Case C.

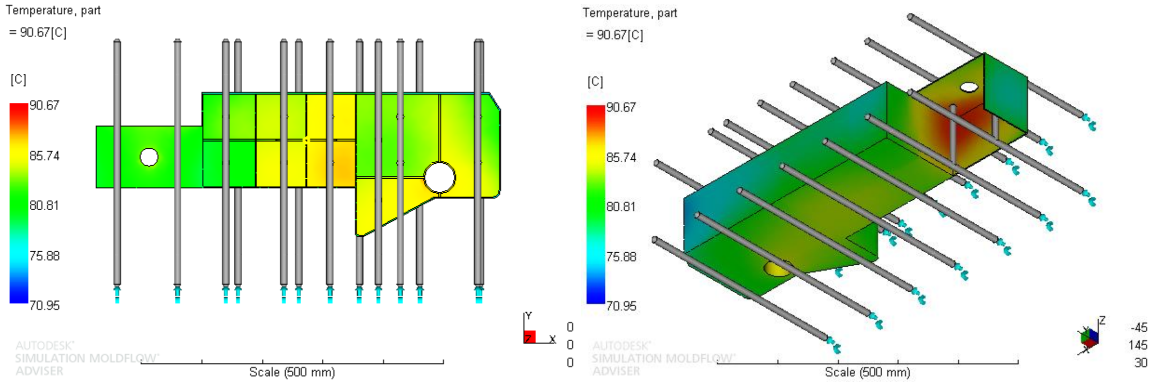

Fig. 32.- Distribution of the average temperature field on the surface of the plastic part during the cooling phase, Case C.

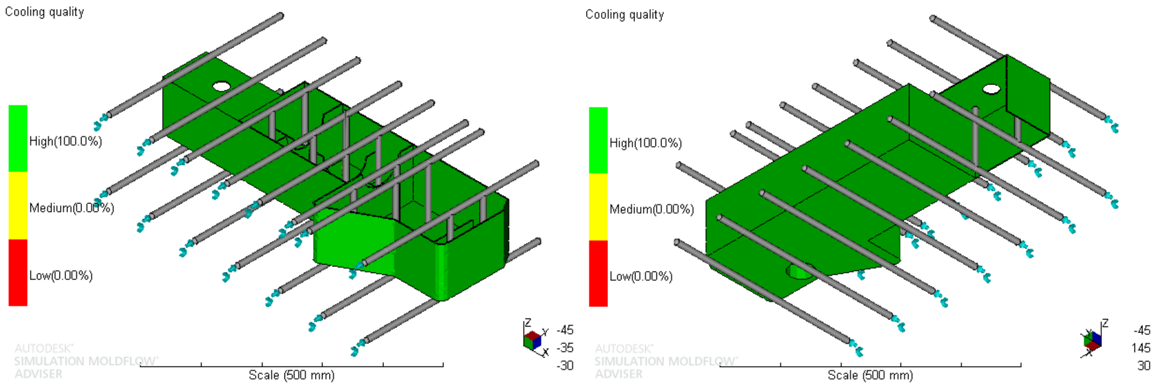

Fig. 33.- Final quality of cooling along the geometry of the plastic part, Case C.

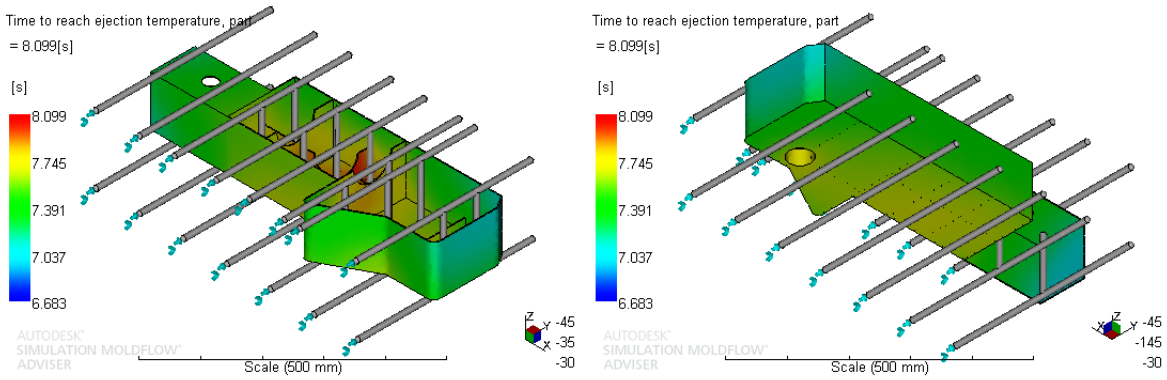

Fig. 34.- Cycle time distribution [s] or time required to reach the ejection temperature on the surface of the plastic part, Case C.

Nomenclature	Units	Description	Analytical algorithm	Injection molding simulation
$\overline{T_m}$	ºC	Average mold cavity surface temperature	77.3	81.6
T_c	ºC	Coolant temperature	67.2	67.0
t_{cycle}	s	Average time required to reach ejection temperature	6.7	7.4
Q	-	Cooling quality	-	100 %
L_b	mm	Distance between baffles	100	100
$D_{baffles}$	mm	Diameter of cooling channels	12	12

Table 9.- Results of the algorithm for Case C: Average mold cavity surface temperature ($\overline{T_m}$) [ºC], coolant temperature (T_c) [ºC], average time required to reach ejection temperature (t_{cycle}) [s], coolant quality, distance between baffles (L_b) [mm] and diameter of cooling channels ($D_{baffles}$) [mm].

4.1.4. Case D

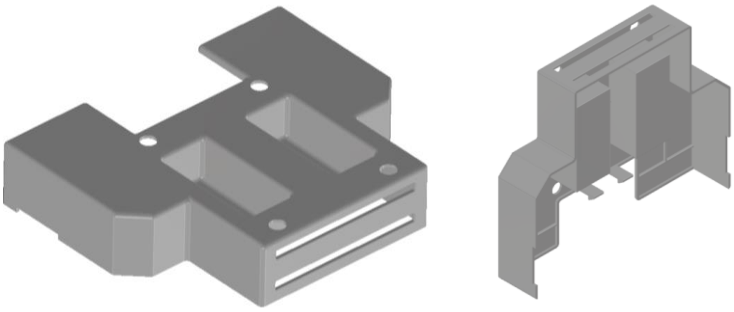

Fig. 35.- Plastic part, Case D.

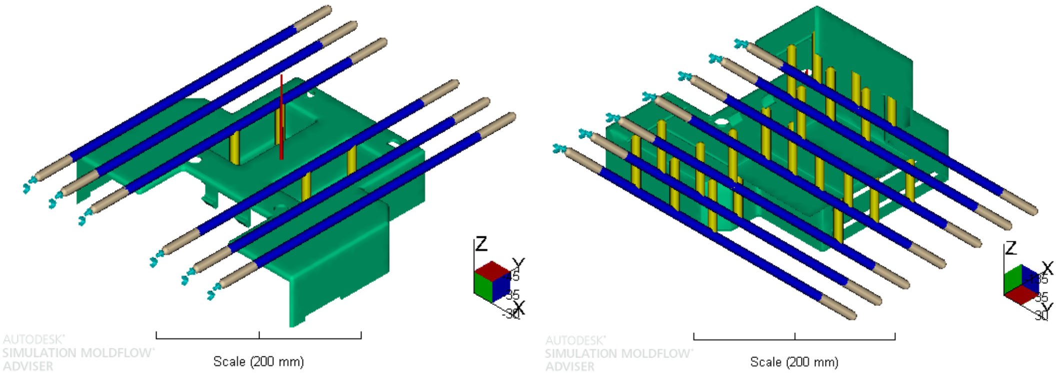

Fig. 36.- Geometric solution of the hybrid refrigeration system design, Case D.

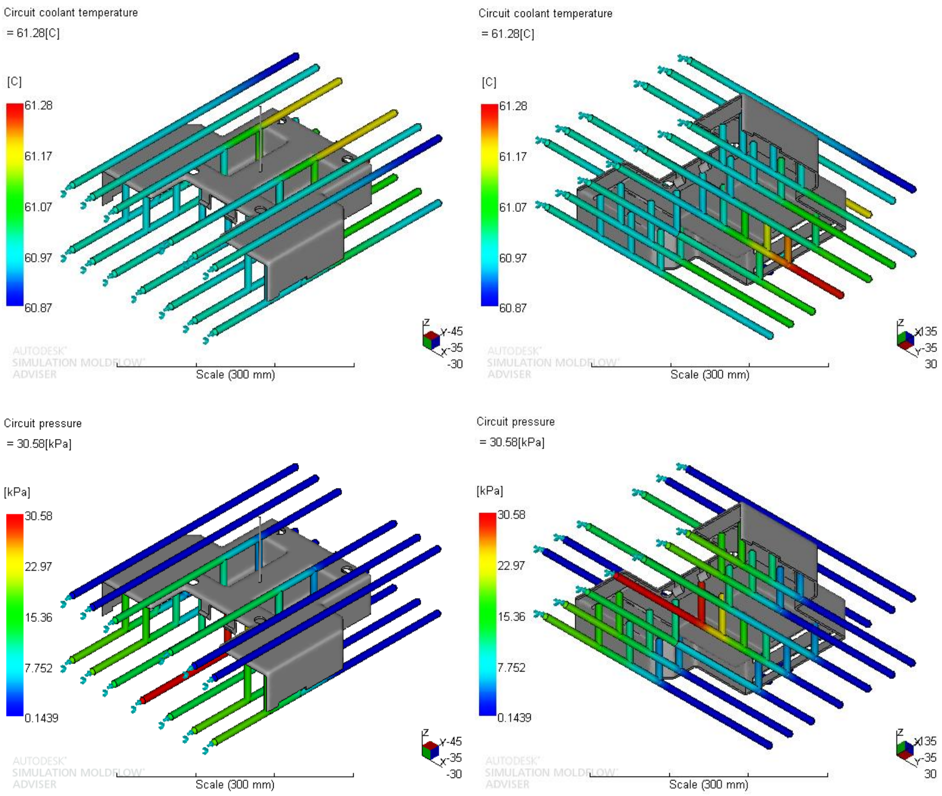

Fig. 37.- Distribution of the pressure field [kPa] and temperatures [° C] of the refrigerant fluid throughout the refrigeration system, Case D.

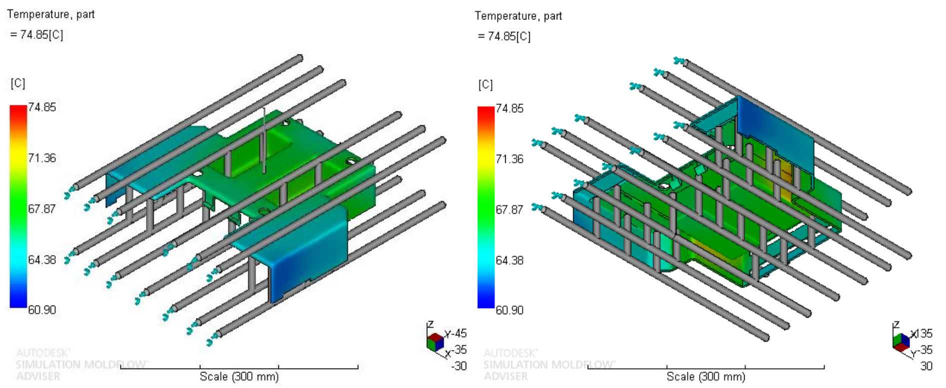

Fig. 38.- Distribution of the mean temperature field at the surface of the plastic part during the cooling phase, Case D.

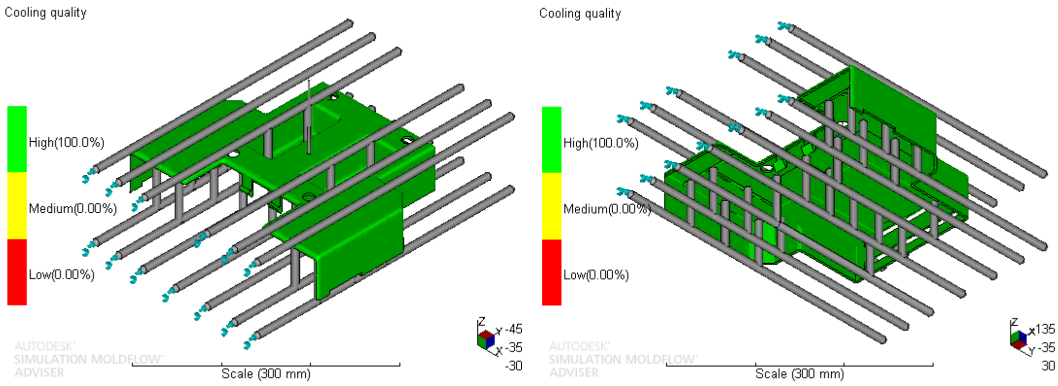

Fig. 39- Final quality of cooling along the geometry of the plastic part, Case D.

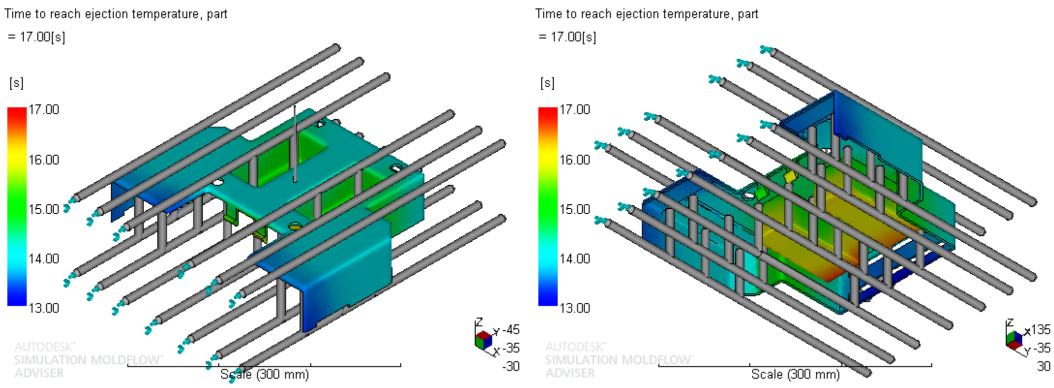

Fig. 40.- Distribution of the cycle time [s] or time required until the ejection temperature is reached on the surface of the plastic part, Case D.

Nomenclature	Units	Description	Analytical algorithm	Injection molding simulation
$\overline{T_m}$	ºC	Average mold cavity surface temperature	67.3	67.9
T_c	ºC	Coolant temperature	61.0	61.0
t_{cycle}	s	Average time required to reach ejection temperature	14.0	14.7
Q	-	Cooling quality	-	100 %
L_b	mm	Distance between baffles	40	40
$D_{baffles}$	mm	Cooling channel diameters	10	10

Table 10.- Results of the algorithm for Case D: Average mold cavity surface temperature ($\overline{T_m}$) [ºC], coolant temperature (T_c) [ºC], average time required to reach ejection temperature (t_{cycle}) [s], coolant quality, distance between baffles (L_b) [mm] and diameter of cooling channels ($D_{baffles}$) [mm].

5. Conclusions

The work presented in this paper shows a new geometric algorithm for automated design of the layout and dimensioning of the baffles and main cooling channels of the cooling system, based on the discrete geometry of the plastic part. The methodology has been tested through its application on four plastic parts with different geometries and dimensions, solving and dimensioning the cooling parameters related to the average mold cavity surface temperature, coolant inlet temperature and cycle time. Location and distribution of main cooling channels and baffles for the four case studies were obtained in an automatic way. Results showed the layout with main cooling channels and baffles on the part. Additionally, a detailed data report is obtained as a result of the application. This report includes the diameter $D_{baffles}$ [mm] and coordinates X, Y, Z of each cooling channel and baffle, the average mold cavity surface temperature $\overline{T_m}$ [ºC], coolant inlet temperature T_c [ºC], cycle time t_{cycle} [s] and distance separation between baffles L_b [mm]. The algorithm of geometric design performs the correct location of the main cooling channels and baffles since the optimization procedure ensures a proper balanced and uniform cooling system, each element of the cooling system is separated from each other at a distance greater than the safety distance D_p [mm] and the location of baffles guarantees the cooling in the regions of the plastic part in which its cooling process is complicated. In addition, the resolution by means of genetic algorithm of the physical model proposed for determining the technical parameters of the cooling system has been validated by means of injection molding software, obtaining results that ensure a high quality of plastic parts during the cooling phase and a cycle time reduction. These are the criteria imposed on the fitness functions that the system must meet.

This new method improves the methods used so far as it does not require heuristic methods to achieve the result and does not use the feature recognition method as a tool for recognizing the geometric surface of the plastic, avoiding the problems of dependence on the modeler and the recognition of complex features. The proposed algorithm is applicable to any geometry because it works regardless of the CAD system in which the part has been designed.

6. Acknowledgements

This work has been supported by the Consejeria de Economia, Innovación, Ciencia y Empleo (Junta de Andalucia-Spain) through the project titled “A vertical design software for integrating operations of automated demoldability, tooling design and cost estimation in injection molded plastic parts. (CELERMOLD)” (Project Code TI-12 TIC 1623). The authors would like to thank the reviewers for comments that improved the exposition.

7. Appendices

7.1. Physical model of the cooling system

The heat transfer model considered in the algorithm focuses on the study of a cooling cell as a way of dimensioning the complete mold cooling system. As shown in Fig 41, the cooling cell consists of a rectangular prism containing a cylindrical baffle. The cooling cells are parameterized geometrically using the values of the diameter of the baffles $D_{baffles}$ [mm], the separation between baffles L_b [mm] and the separation between the blend of the baffle and the plastic part L_p [mm] (See Fig 41).

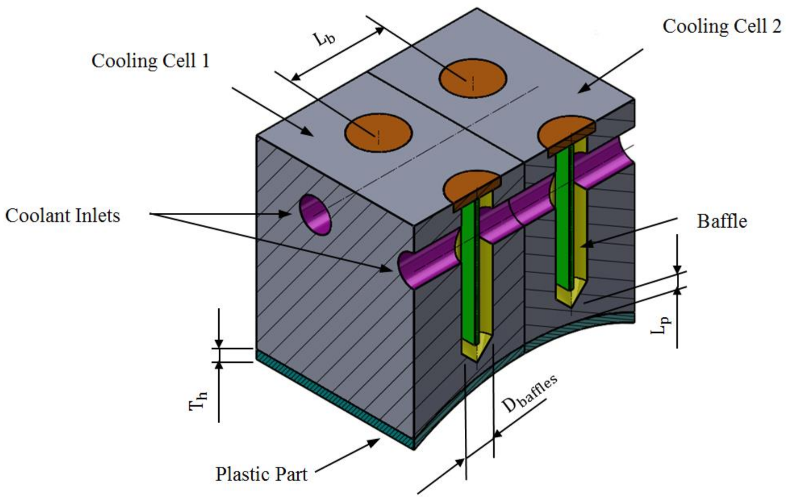

Fig. 41.- Cooling cell considered for the dimensioning of the complete mold.

In the physical model of heat transfer between the plastic part and the cooling system, a series of premises have been taken into account with the aim of mathematically simplifying the physical model, Park et al. [31].

- The physical properties of the metal material in the mold are constant.
- The thermal analysis of the melt polymer is considered unidirectional because the thickness of the mold is smaller than the planar dimension.
- Heat exchange between the mold and the outside medium by convection is neglected because it represents less than 5% of overall heat loss.
- The cycle time of the plastic part is assumed equal to packing & cooling time because the filling and the ejection time are substantially shorter than packing & cooling time.
- It is assumed that the flow rate of coolant is large enough to achieve effective turbulent flow.
- The cooling effect of the main cooling channels is included in those regions of the part which do not require baffles.

According to Xu et al. [19], the steady state cycle mold cavity surface temperature, denominated as $\overline{T_m}$ [ºC], can be expressed as Eq.(38).

$$\overline{\mathrm{T_m}} = \mathrm{T_c} + \frac{\rho_\mathrm{p} \cdot \mathrm{c_p} \cdot \mathrm{T_h} \cdot \left(2 \cdot \delta_\mathrm{s} \cdot \mathrm{L_b} + \mathrm{h} \cdot \pi \cdot \mathrm{D_{baffles}} \cdot \mathrm{L_p}\right) \cdot (\mathrm{T_{melt}} - \mathrm{T_{eject}})}{\mathrm{h} \cdot \pi \cdot \mathrm{D_{baffles}} \cdot \delta_\mathrm{s} \cdot \mathrm{t_{cycle}}} \tag{38}$$

Where T_c [ºC] represents the temperature of the coolant, ρ_c [kg/mm^3] represents the density of the melt plastic, c_p [J/kg·ºC] represents the specific heat of the melt plastic, T_h [mm] represents the thickness of the plastic part, δ_s[W/mm·ºC] represents the thermal conductivity of the mold, L_b [mm] represents the separation between baffles, h [W/mm^2·ºC] represents the heat transfer coefficient between the mold and the coolant, $D_{baffles}$ [mm] represents the diameter of the baffles, L_p [mm] represents the separation between the plastic part and the baffle for a cooling cell, T_{melt} [ºC] represents the melt plastic temperature, T_{eject} [ºC] represents the temperature of ejection of the part (characteristic of each polymer) and t_{cycle} [s] represents the cycle time of the plastic part.

This expression allows estimation of the temperature of the surface of the mold cavity; however it is necessary to know the value of the cycle time t_{cycle} [s], since it is an input variable to the model. The cycle time can be defined from the equation that determines one-dimensional heat flow Eq.(39), i.e. the Fourier equation reduced to one dimension. According to Menges et al. [33].

$$\frac{\partial \mathrm{T}}{\partial \mathrm{t}} = \alpha_\mathrm{s} \cdot \frac{\partial^2 \mathrm{T}}{\partial^2 \mathrm{z}} \tag{39}$$

Where α_s [m^2/s] represents the thermal diffusivity coefficient of the mold material. Assuming that, after the filling stage of the mold cavity, the melt plastic temperature has a constant value T_{melt} [ºC] and the surface temperature of the mold cavity varies considerably until it remains at a constant value $\overline{T_m}$ [ºC], a solution can be established to this second-order and hyperbolic differential equation Eq.(40). The melt plastic temperature at a point on the partition line can be evaluated as a convergence of the Fourier series development of the heat transfer differential equation, such that.

$$\frac{\mathrm{T_{eject}} - \overline{\mathrm{T_m}}}{\mathrm{T_{melt}} - \overline{\mathrm{T_m}}} = \frac{4}{\pi} \mathrm{e}^{-\frac{\alpha_\mathrm{s} \cdot \pi^2}{\mathrm{T_h}} \cdot \mathrm{t}} \cdot \sin\left(\frac{\pi \cdot \mathrm{x}}{\mathrm{S}}\right)$$

$$\mathrm{T_{eject}} - \overline{\mathrm{T_m}} = \frac{4}{\pi} \cdot (\mathrm{T_{melt}} - \overline{\mathrm{T_m}}) \cdot \sum_{\mathrm{n}=0}^{\infty} \frac{1}{2 \cdot \mathrm{n} + 1} \cdot \mathrm{e}^{-\frac{\alpha_\mathrm{s} \cdot (2 \cdot \mathrm{n}+1) \cdot \pi^2}{\mathrm{T_h^2}} \cdot \mathrm{t}} \cdot \sin\left(\frac{\pi \cdot (2 \cdot \mathrm{n} + 1) \cdot \mathrm{x}}{\mathrm{S}}\right) \tag{40}$$

Resolving the above expression with respect to the cycle time Eq.(41).

$$\mathrm{t_{cycle}} = \frac{\mathrm{T_h^2}}{\pi^2 \cdot \alpha_\mathrm{s}} \cdot \mathrm{Ln}\left(\frac{4}{\pi} \cdot \frac{\mathrm{T_{melt}} - \overline{\mathrm{T_m}}}{\mathrm{T_{eject}} - \overline{\mathrm{T_m}}}\right) \tag{41}$$

Thus, in the expression the cycle time is a function of the temperature of the surface of the mold cavity and vice versa. Authors such as Xu et al. [19] proposed the resolution of this model through an iterative process of calculation. Wang et al. [27, 28] assigned values of the diameter of the cooling channels and cycle time based on the industrial experience and calculated the other technical and geometric parameters of the physical model. However, models [19, 27, and 28] present problems in their complete resolution, and for this reason the algorithm proposed in this paper employs a genetic optimization algorithm that calculates the optimal technical and geometric parameters of the physical model.

7.2. Flowchart of the present methodology

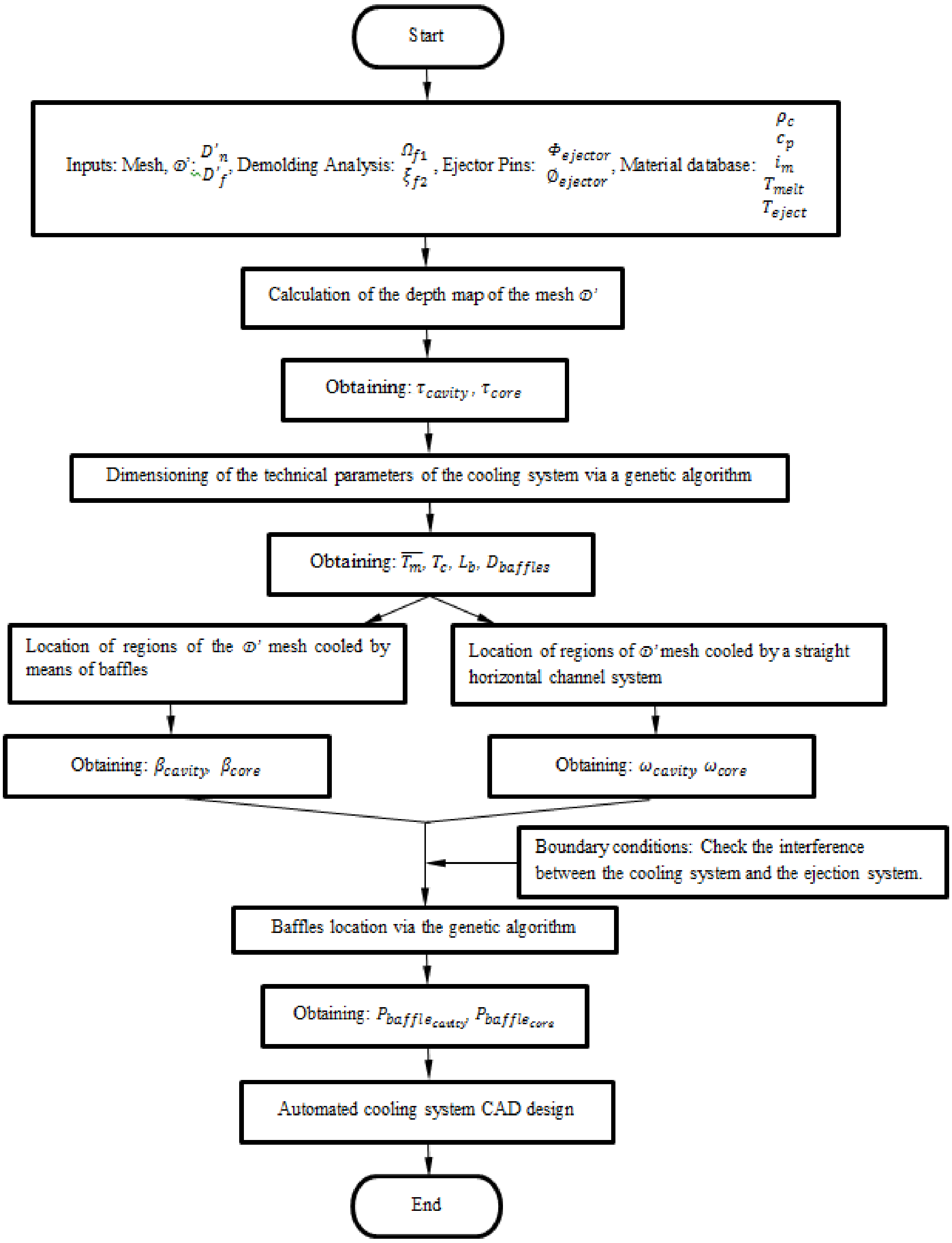

Fig. 42.- Algorithm for the design and dimensioning of the injection mold cooling system.

8. Bibliography

[1] C. Martin- Doñate, M.A. Rubio Paramio. New methodology for demoldability analysis based on volume discretization algorithms. Computer-Aided Design 2013: 45: 2: 229-240

[2] Jorge Manuel Mercado-Colmenero, M.A.R. Paramio, Jesus Maria Perez-Garcia, Cristina Martin-Doñate. A new hybrid method for demoldability analysis of discrete geometries . Computer- Aided Design. 2016 : 80: 43–60.

[3] Cristina Martin-Doñate, Miguel Angel Rubio-Paramio, Aurelio Mesa-Villar. Método de validación automatizada de la fabricabilidad de diseños de objetos tridimensionales en base a su geometría 2015, Patent number: ES2512940B2

[4] M.A. Rubio,J.M. Pérez, J. Rios, A Procedure for Plastic Parts Demoldability Analysis Robotics and Computer Integrated Manufacturing, 2006:22:1:. 81–92.

[5] Turng, L S Wang, K K A computer-aided cooling-line design system for injection molds. Journal of Engineering for Industry-Transactions of the ASME 1990: 112: 2 : 161-167

[6] Opolski SW, Kwon TW. Injection molding cooling system design. ANTEC'86 1987 pp 264-268.

[7] Tang LQ, Pochiraju K, Chassapis C, Manoochehri S. A computer- aided optimization approach for the design of injection mold cooling systems. Trans of ASME Journal of Mechanical Design 1998;120:165-74.

[8] Sanfilippo EM, Borgo S. What are features? An ontology-based review of the literature. Computer-Aided Design In Press, Corrected Proof, Available online 14 July 2016

[9] Li CL. A feature-based approach to injection mould cooling system design. Computer-Aided Design 2001; 33(14):1073–90.

[10] Li CL, Li CG, Mok ACK. Automatic layout design of plastic injection mould cooling system. Computer-Aided Design 2005; 37(7):645–62.

[11] Li CG, Li CL. Plastic injection mould cooling system design by the configuration space method. Computer-Aided Design 2008; 40(3):334–49.

[12] Li C.G,. Li C.L, Liu Y., Huang Y. A new C -space method to automate the layout design of injection mould cooling system. Computer-Aided Design 2012; 44():812–423.

[13] Sachs E , Wylonis E, Allen S, Cima M ; Guo HL., Production of injection molding tooling with conformal cooling channels using the three dimensional printing process. Polymer Engineering and Science.2000;40(5):1232-1247

[14] Dalgarno KW; Stewart TD. Manufacture of production injection mould tooling incorporating conformal cooling channels via indirect selective laser sintering. Proceedings of the Institution of Mechanical Engineers Part B-Journal of Engineering Manufacture 2001; 215 (10):1323-1332

[15] Ilyas I.; Taylor C.; Dalgarno K.; et ál. Design and manufacture of injection mould tool inserts produced using indirect SLS and machining processes. Rapid Prototyping Journal. 2010; 16 (6) : 429-440

[16] Ferreira, JC; Mateus, A; Studies of rapid soft tooling with conformal cooling channels for plastic injection moulding. Journal of Materials Processing Technology 2003;142(2) :508-516 .

[17] Saifullah, A. B. M.; Masood, S. H.; Sbarski, I. Thermal-structural analysis of bi-metallic conformal cooling for injection moulds. International Journal of Advanced Manufacturing Technology 2012; 62 (1-4) : 123-133

[18] Eiamsa-ard K.; Wannissorn K.: Conformal bubbler cooling for molds by metal deposition process. Computer-aided design 2015 69 (): 126-133

[19] Xu, XR; Sachs, E; Allen, S. The design of conformal cooling channels in injection molding tooling. Polymer engineering and science. 2001. 41(7) 1265-1279

[20] Dimla, DE; Camilotto, M; Miani, F. Design and optimisation of conformal cooling channels in injection moulding tools. Journal of Materials Processing Technology 2005 164: 1294-1300

[21] Qiao, H. A systematic computer-aided approach to cooling system optimal design in plastic injection molding. International Journal of Mechanical Sciences 2006; 48 (4) 430-439.

[22] Au, K. M.; Yu, K. M. A scaffolding architecture for conformal cooling design in rapid plastic injection moulding. International Journal of Advanced Manufacturing Technology. 2007 34 (5-6) 496-515.

[23] Park, H. S.; Pham, N. H. Design of conformal cooling channels for an automotive part. International journal of automotive technology. 2009; 10(1) : 87-93

[24] Au, K. M.; Yu, K. M. Modeling of multi-connected porous passageway for mould cooling. Computer-Aided Design 2011; 43(8) : 989-1000.

[25] Au, K. M.; Yu, K. M.; Chiu, W. K. Visibility-based conformal cooling channel generation for rapid tooling. Computer-Aided Design 2011; 43(4) 356-373.

[26] Au, K. M.; Yu, K. M. Variable Distance Adjustment for Conformal Cooling Channel Design in Rapid Tool. Journal of Manufacturing Science and Engineering-Transactions of the ASME. 2014; 136 (4)

[27] Wang, Yu; Yu, Kai-Min; Wang, Charlie C. L. et ál. Automatic design of conformal cooling circuits for rapid tooling. Computer-Aided Design 2011; 43(8):1001-1010.

[28] Wang, Yu; Yu, Kai-Min; Wang, Charlie C. L. Spiral and conformal cooling in plastic injection molding. Computer-Aided Design 2015; 63() 1-11

[29] Sun, YF; Lee, KS; Nee, AYC. The application of U-shape milled grooves for cooling of injection moulds. Proceedings of the Institution of Mechanical Engineers Part B-Journal of Engineering Manufacture 2002; 216 (12) 1561-1573.

[30] Dang, Xuan-Phuong; Park, Hong-Seok. Design of U-shape Milled Groove Conformal Cooling Channels for Plastic Injection Mold. International Journal of Precision Engineering and Manufacturing. 2011. 12 (1) 73-84 .

[31] Park, HS , Dang, XP .Optimization of conformal cooling channels with array of baffles for plastic injection mold International Journal of Precision Engineering and Manufacturing. 2010.11(6) 879-890.

[32] Jorge Manuel Mercado-Colmenero, M.A.Rubio- Paramio, Antonio Vizan-Idoipe, Cristina Martin-Doñate. A new procedure for the automated design of ejection system in injection molds. Robotics and Computer Integrated Manufacturing 2017:46:68-85

[33] G. Menges, P. Mohren, How to Make Injection Moulds, 3rd ed., Hanser, Munich, Vienna and New York, 2001.

[34] Kazmer , David, Injection Mold Design Engineering, 1st ed., Hanser, Munich 2007.

[35] Matlab, R2013a. https://mathworks.com

[36] Autodesk, MoldFlow Advisor, 2014. http://www.autodesk.com

Vitae

Jorge Manuel Mercado Colmenero received his B.Eng and M.Eng. in Mechanical Engineering in 2012 and 2014 respectively from the University of Jaén in Spain. In 2014 he joined the Design, Engineering Graphics and Project department at Jaen university as a PhD student. He is currently developing his thesis on automatic analyses and design of injection plastic molds, including demoldability, ejection systems, cooling system design and CAD-CAE design and manufacturing.

Dr. Miguel Angel Rubio Paramio received his MEng and Ph.D in Mechanical Engineering in 1992 and 2000 respectively from the Polytechnic University of Madrid in Spain. In 1994 he joined the University of Jaen and currently he teaches courses on Computer-aided Design, Manufacturing and Engineering in the Engineering Graphics, Design and Projects Department. His thesis was focused on the automatic analysis of plastic parts injection. His research interests include CAD-CAM-CAE, Design for Manufacturing, computational geometry, constraint-based parametric modeling, and their applications in plastic injection mold design and manufacturing.

Prof. Dr. Marquez received his Msc and Ph.D. degrees in Mechanical Engineering from Universidad Politecnica of Madrid (UPM, Spain) in 1994 and 1998, respectively. He is currently a full time Professor in the Dep. of Mechanical Engineering at ETSII-UPM. His research work focuses on the design and development of high precision manufacturing systems and polymer microfabrication technologies. He has led two research projects in the area of MEMS micromanufacturing, and he has participated as associate researcher in many others. He has been visiting professor at the George W. Woodruff School of Mechanical Engineering at Georgia Institute of Technology (USA) in 1996,2005 and 2009, collaborating in research groups at the Manufacturing Research Center. He has been on the position as Vice-Dean for Students Affairs and International Relations since 2011 at ETSII-UPM.

Dr. Cristina Martín - Doñate received her B.Eng. and M.Eng. in Electrical - Electronics Engineering and Industrial Engineering (Polytechnic University of Valencia - Spain) and Ph.D in Industrial Engineering (University of Jaen - Spain) in 1997 and 2010 respectively. She performed research at the Technical University of Graz in Austria, in the field of manufacturing systems. She worked for several years as a project manager developing new products in the automotive manufacturing industries. She is currently Full Professor at Jaen University where she develops research and conducts research projects into manufacturing systems, plastic injection mold design and technology, CAD systems and new products development.